Heliyon 10 (2024) e38789

Contents lists available at ScienceDirect

Heliyon

journal homepage: www.cell.com/heliyon

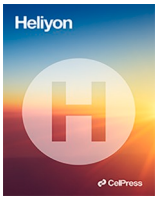

Research article

Spatial and seasonal variability of chlorophyll-a, total suspended matter, and colored dissolved organic matter in the Sundarban mangrove forest using earth observation and field data

Mosa. Tania Alim Shampa [a], Md. Kawser Ahmed [a], K. M. Azam Chowdhury [a], Md. Ashraful Islam [b], Mahmudul Hasan [a,*], Muhammad Shahinur Rahman [c], Md. Saiful Islam [d]

[a] *Department of Oceanography, University of Dhaka, Dhaka, 1000, Bangladesh*
[b] *Department of Geology, University of Dhaka, Dhaka, 1000, Bangladesh*
[c] *Physical and Space Oceanography Department, Bangladesh Oceanographic Research Institute, Cox's Bazar, 4700, Bangladesh*
[d] *Department of Soil Science, Patuakhali Science and Technology University, Dumki, Patuakhali, 8602, Bangladesh*

ARTICLE INFO

Keywords:
Sundarban mangrove
Health of aquatic environment
Chlorophyll-a (Chl-a)
Total suspended matter (TSM)
Colored dissolved organic matter (CDOM)
Ocean Color algorithm

ABSTRACT

The Sundarbans, the world's largest mangrove forest, confronts potential threats from various anthropogenic activities leading to degradation of its aquatic ecosystem. To examine the current status of the aquatic ecosystem, this study aimed to evaluate the spatial and seasonal fluctuation of three principal water quality attributes namely Chlorophyll-a (Chl-a), Total Suspended Matter (TSM), and Colored Dissolved Organic Matter (CDOM) in the complex tidal river systems of the Sundarban mangroves forest using earth observation and in-situ data. A set of two bio-optical algorithms, Ocean color-2 (OC-2) and Ocean color-3 (OC-3), were applied to measure Chl-a concentration, Green/NIR and the Red/NIR band ratio algorithms were used for TSM and the Case-2 Regional Coast Color (C2RCC) processor in the SNAP software was applied to obtain CDOM concentration in study area. A total of 50 in-situ samples were collected during post-monsoon and pre-monsoon to validate the results. Our results clearly demonstrated seasonal variability with higher Chl-a concentrations in post-monsoon than pre-monsoon. This was due to the OC-2 algorithm which produced better results with $R^2 = 0.73$, RMSE = 0.27 for post-monsoon and $R^2 = 0.55$, RMSE = 0.32 for pre-monsoon. Whilst, TSM concentration performed the best with $R^2 = 0.77$; RMSE = 15.82 and $R^2 = 0.65$; RMSE = 33.96 in post-monsoon and pre-monsoon according to the Green/NIR band ratio method. The nearshore and narrow waterway regions had the highest concentrations of TSM and Chl-a, whereas the offshore regions had the lowest. Strong association were observed between the in-situ and satellite derive absorption coefficient, a^{CDOM} (m^{-1}). The R^2 for a CDOM during pre-monsoon was 0.65 and throughout the post-monsoon, it was 0.74. Pre-monsoon concentrations were found to be higher due to marine sources and higher wind speeds, possibly due to sediment resuspension. This kind of baseline evaluation will help to detect threats, direct preventive measures for the protection of biodiversity, and deepen our knowledge of these distinct ecosystems. The results will help develop flexible management and preservation plans that can adjust to both natural and man-made changes.

* Corresponding author.
E-mail address: mahmud.hasan@du.ac.bd (M. Hasan).

https://doi.org/10.1016/j.heliyon.2024.e38789
Received 14 July 2024; Received in revised form 27 September 2024; Accepted 30 September 2024
Available online 2 October 2024

1. Introduction

The Sundarbans, the world's largest mangrove forest, acts as an exceptionally productive ecosystem, profoundly influenced by the substantial nutrient flow from the intersecting rivers within the region [1–5]. The Sundarbans ecosystem, situated with the Ganges deltaic system spanning both the territory of Bangladesh and India, presents unparalleled biodiversity [6] and playing a pivotal role, in serving as a vital breeding area for numerous economically significant fish species [7–9]. The intricacies of this mangrove ecosystem play a significant role in maintaining a strong fishing productivity, holding crucial importance for coastal communities, particularly those grappling with economic difficulties [10]. These coastal marine fisheries not only offer essential livelihood opportunities but also make substantial contributions to national economic growth ensuring food nutrition security [10]. Moreover, this ecosystem contributes a huge source of sustenance for local residents by providing resources such as honey, wood, timber and non-timber forest product, tourism [11]. Despite the valuable benefits it provides to local communities, the Sundarbans ecosystem is currently facing deterioration and is at potential risk, particularly in terms of its aquatic environment. A range of anthropogenic activities, including pollution, oil spills, plastic debris, heavy metal contamination, sewage [12,13], industrial wastewater discharge, agricultural runoff, collectively exert a detrimental impact on the health, diversity, productivity, and functioning capabilities of the Sundarban ecosystem [4,14]. The primary productivity of the Sundarbans ecosystem is significantly shaped by the inflow of nutrients and debris from river, the excess nutrients released from wastewater into coastal waterways lead to eutrophication and hypoxia, resulting in phytoplankton blooms [14–16]. Hazardous algal blooms, which reduce oxygen levels, impede light penetration, and block fish gills [107]. The Sundarbans and the areas around them are quite busy because of the operation of multiple commodities and vessels. For example, the area around Mongla Port is facing problems with the manufacturing of various wastes [17]. Events like oil leaks during port loading and unloading and infiltration into the oceans exacerbate this issue even more [18]. These activities reduce the amount of sunlight that reaches deeper waters, which eventually reduces photosynthesis and ecosystem productivity in the Sundarbans. Oil pollution in the Sundarbans has been shown to have a significant impact on the number of plankton communities and water quality [19]. Such actions weaken the aquatic ecosystem's ability to support productivity and pose a major threat to it. To be able to attain maximum benefit from ecosystem and also be able to protect its environment baseline status it is necessary to determine the impact of anthropogenic threats on the primary productivity, ecosystem function, biogeochemical cycles, bio-geochemistry, and water quality of the coastal waters in the Sundarbans mangrove forest. Therefore, the main goal is thought to be assessment and monitoring in order to protect this delicate aquatic habitat from further deterioration. Water quality metrics including Chl-a, TSM, and CDOM have been utilizing extensively and successfully to determine the health of aquatic ecosystems [20]. Chl-a serves as a proxy for phytoplankton biomass, indicating higher concentrations in environments with increased phytoplankton, leading to plankton blooms as a form of coastal pollution [21]. TSM comprises solid particles like organic and inorganic matter, algal detritus, and various organisms suspended in water, influencing the underwater ecological function by affecting light distribution and optical properties [22–25]. CDOM, a fraction of dissolved organic matter , absorbs photo-synthetically active radiation, impacting productivity at different depths and providing UV protection [26]. Its entry into aquatic environments occurs through plant and animal decomposition, affecting water color and influencing upper and underwater primary productivity [27]. Chl-a, TSM, and CDOM are naturally or anthropogenic ally occurring optically active substances with light-absorbing and scattering characteristics in the ultraviolet and visible spectrum [28–30]. These substances impact total primary productivity and fish abundance in near-shore environments [31].

Thus, by measuring the water leaving radiance in the visible spectrum of electromagnetic radiation [31], an accurate measurement of Chl-a, TSM and CDOM is required for the assessment of water quality, monitoring the level of pollution and its seasonal variability [32,33], primary productivity, ecological functioning and the sustainability of the aquatic environment. Water quality needs to be monitored continuously, although the conventional in-situ observations provide accurate measures but labor-intensive, time consuming and time series monitoring is impractical [34]. Hence, satellite remote sensing provides a through foundation for long-term, continuous water quality monitoring. It is the most effective way to find out how these parameters are distributed in the coastal area both seasonally and spatially.

Earth observation data plays a pivotal role in monitoring and assessing aquatic environments [35,109]. Utilizing satellite imagery and remote sensing technologies, scientists can gain valuable insights into the health and dynamics of water bodies and represent them in a spatially explicit way [36–39]. By employing spectral indices and algorithms, water quality parameters such as Chl-a concentration, TSM, and CDOM [40] can be measured spatially enabling researchers to identify trends, spatial patterns, and potential environmental stressors impacting aquatic ecosystems [35,41]. The ability to conduct temporal analyses facilitates the detection of changes over time, aiding in the assessment of long-term trends or the impact of human activities and climate change [42]. Earth observation data analysis, coupled with ground validation, has been employed in many studies as a potent tool for informed decision-making in environmental management, conservation initiatives, and the sustainable use of aquatic resources [43,44].

Given its significance, this approach has been applied in numerous studies so far across the globe. For instance, Poddar et al. (2019) [45] employed Landsat-8 and Sentinel-2 satellite imagery to estimate Chl-a concentrations in the Bay of Bengal (BoB); Kyryliuk and Kratzer [46] utilized the C2RCC method to estimate water quality parameters in the Baltic Sea, employing Sentinel-3 satellite data; Das et al. (2017) [47] measured concentrations of CDOM in the northern BoB; while De et al. (2021) [48] focused on estimating Chl-a and SPM using Sentinel-3 satellite data along the northeast coast of the BoB; Moutzouris-Sidiris and Topouzelis (2018) [49] employed Sentinel-2 satellite data for Chl-a estimation; Ouma et al. (2020) [50] investigated Chl-a, TSS, and turbidity using Sentinel-2 MSI and Landsat-8 OLI, employing a multivariate regression model; Boucher et al. (2018) [51] studied Chl-a estimation using Landsat-8, Watanabe et al. (2017) [52] estimated Chl-a using Landsat-8 OLI and Sentinel-2 MSI sensors; and Salyuk et al. (2022) [53] applied a bio-optical algorithm to remote sensing techniques in the western part of the Bering Sea. Although few researches are evident in

Sundarban areas, however, a comprehensive studies targeting major water quality parameters have not been attempted so far.

Since the Sundarbans mangrove forest is acknowledged globally as the most significant ecosystem, the ecology of the mangroves warrants protection by routine monitoring and assessments of water quality. Considering this fact and address the research gap, this study thus intended to evaluate water quality parameters in Sundarban areas to be able to investigate seasonal variability of the health of aquatic environment using multi-temporal earth observation and in-situ data. We utilized Sentinel-2 MSI and Landsat-8 OLI due to their higher spatial resolution provide regular and consistent observations over a large area, and they are also effective for monitoring water quality, inherent optical properties, and sediment transport, as well as analyzing the fate and distribution of these parameters in riverine and coastal water [54,55]. Therefore, the main objectives of this research are i) to analyze the seasonal variability and spatial distribution of Chl-a, TSM, and CDOM ii) To validate the satellite derived Chl-a, TSM, and CDOM with in-situ data iii) To evaluate the appropriate algorithm to retrieve Chl-a, TSM, and CDOM iv) spatial distribution of these parameters in the study area using geospatial techniques. This study thus helps to get information about the land based marine pollution (HABs, eutrophication), potential productive fishing zones, and the health of the ecosystems in order to take necessary actions for strengthening their resiliency, protection, and restoration so that the country can reach the SDG goal 14.

2. Materials and methodology

2.1. Study area

The Sundarbans is a vast mangrove forest located in the southwestern tip of the Ganges delta is believed to be formed by the confluence of several rivers, including the Ganges, Brahmaputra, and Meghna [56]. Majority of its aerial coverage is in Bangladesh (60%) that stretches into India (40%) on the western side [57]. The Sundarban was declared a UNESCO World Heritage Site in 1997 and a Ramsar Wetland Site by the Ramsar Convention in 2007 [58]. The region is characterized by a complex network of tidal waterways, small islands, mudflats, and dense mangrove forests [59]. Being the largest mangrove ecosystem in the world, this ecosystem offers a unique biodiversity hotspot and ecological value [60,108]. This region provides significant ecosystem benefits that sustain the livelihoods of the local population, fostering diverse biodiversity and making essential contributions to the well-being and cultural activities in the neighboring areas [61]. Sundarbans offer elevated primary productivity resulting from nutrient enrichment, making it excellent fishing grounds and breeding ground for various globally threatened species [2,5]. Therefore, the livelihoods of those who live close to the Sundarbans ultimately depend largely on aquaculture, fishing, honey harvesting, agriculture, and fuelwood [62,63].

As for example, fishery production in Sundarbans has risen to 0.18 lakh M.T., contributing 0.42% to the total production and

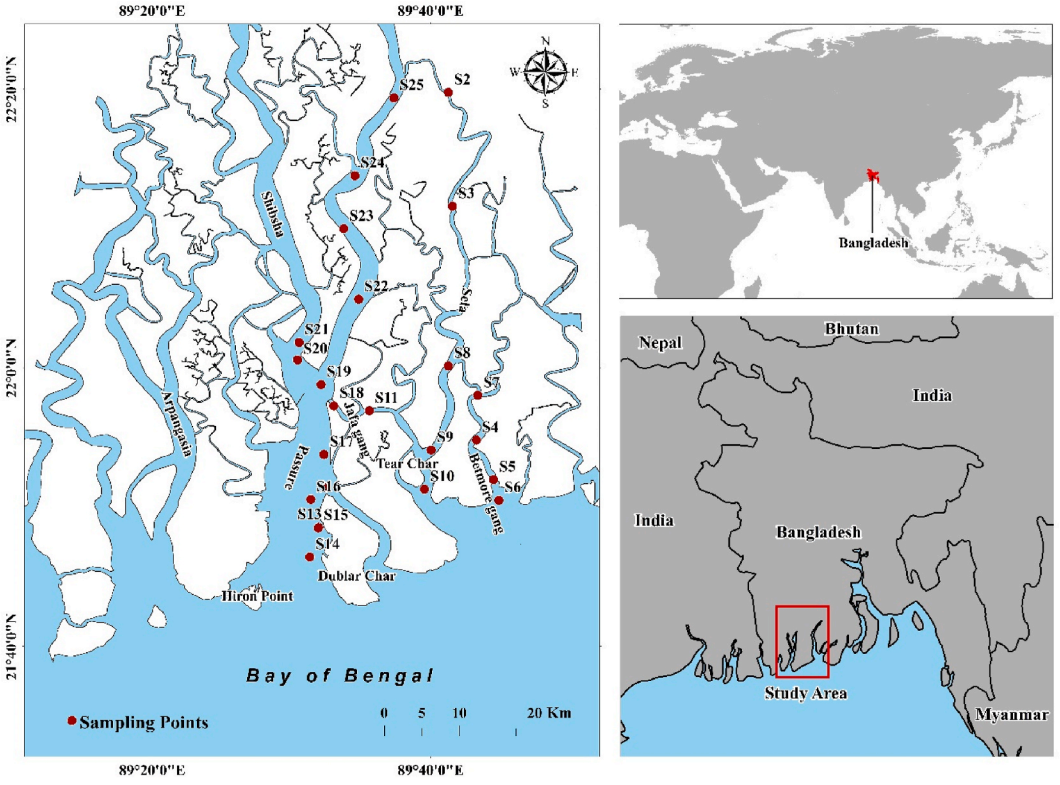

Fig. 1. Location of the study area.

reflecting a growth rate of 0.32% [64]. The fisheries sector contributes 3.52% of the GDP of Bangladesh [64]. Contribute to the national economy, provide food and nutrition security [10], and contribute direct and indirect income as well as employment to 1.7 million individuals residing in the border villages of the Sundarbans [65] and supplies various ecosystem services that benefit approximately 3.5 million people [66]. The Sundarbans ecosystem plays a crucial role in land reclamation, coastal habitat protection from cyclones, and socioeconomic upliftment for coastal communities [14]. But over time, the once-pristine mangrove has seen environmental deterioration [67]. Human-induced factors contributing to the degradation involve diverting freshwater from the Ganges at Farakka, oil pollution, navigation, industrial pollutants, coal-fired power plant construction, heavy metals, pesticides, shrimp cultivation, poaching etc. Pollutants accumulated during dry periods are subsequently washed and transported to the BoB during the monsoon [57]. Besides, over time, unregulated fishing, excessive harvesting of aquatic resources, and habitat destruction disrupt the overall health of the ecosystem.

2.2. In situ data

One of the primary targets of the study was to conduct a comprehensive field investigation to collect samples from the surface of the water across the study area. To do so, we took samples targeting two seasons: i) post-monsoon (12–15 December 2021) ii) pre-monsoon (13–15 April 2022) to be able to assess water quality within the coastal water of the Sundarban's. A total of 50 water samples were collected using Niskin Bottle Sampler from the rivers of Passur, Shibsha, Sela, Jafa Gang, and Betmore Gang of the Sundarban mangrove forest (Fig. 1). In addition, a number of hydrological parameters such as temperature, dissolved oxygen, salinity, pH, total dissolve solid, conductivity, and Secchi disk depth (cm) were measured using a multi-parameter water quality meter during the field data collection. To avoid the water sample's original features being altered by sunlight, some precautions were taken. As soon as the necessary hydrological parameters are measured, we quickly pour the sample water into a sample bottle. Since the parameter that would be examined later is very sensitive to sunshine, we then stored the water samples in an icebox covered in black polythene to protect them from sunlight. After that, a laboratory analysis was accomplished.

2.3. Laboratory estimation of Chl-a, TSM and CDOM

The procedure developed by Marker et al. (1980) [68], which involved double extraction with hot and cold treatments for assessing Chl-a concentrations. The quantification is performed through spectrophotometry, employing 90 % ethanol as the extracting solvent and 2M hydrochloric acid (HCl) in subsequent stages. TSM was quantified in accordance with APHA (2005) [69] gravimetric method. While CDOM measurements were followed by Das et al. (2017) [70]. Finally, the calculation of Chl-a, TSM, and CDOM concentrations were completed using the following equations(1)–(3) in Table 1.

2.4. Multispectral satellite imagery and preprocessing

For our study, we deployed Landsat-8 OLI and Sentinel-2 MSI satellite sensors. The Landsat-8 OLI and Sentinel-2 MSI images were acquired from the Earth Explorer websites (https://earthexplorer.usgs.gov/). All imagery was extracted with a synchronization of the satellite passing time over the area and our sampling time in various spots in the Sundarbans (Table 2). Before using the final imagery, we deployed a few image processing techniques to be able to achieve the best outcomes. The level-1 data from Sentinel-2 MSI is the Top of the Atmosphere (TOA) reflectance, and the level-1 data from Landsat-8 OLI consists of quantized and calibrated scaled DN values. To be able to retrieve Chl-a, TSM, and turbidity from satellite sensors over the study area, we deployed four fold steps [45]. 1) Conversion of scaled DN values to absolute TOA reflectance for all the required bands 2) Conversion of TOA reflectance to bottom of the Atmosphere (BOA) reflectance, BOA is the surface reflectance that actually originates from the water surface. 3) Conversion of the BOA surface reflectance to the corresponding remote sensing reflectance (Rrs) at these bands by dividing the BOA reflectance by π, following the method outlined by Moses et al. (2015) [71]. 4) Using a specific algorithm, retrieve Chl-a and TSM from Rrs. To ensure spatial consistency among the processed imagery we used image to image geo-referencing techniques.

2.5. Retrieval algorithm of Chl-a, TSM and CDOM

Over recent years, several algorithms have been developed to estimate Chl-a from satellite reflectance data, including OC2v2, OC3, Global Processing, and Morel's versions 1–4 [72]. The OC-2 algorithm, initially designed for SeaWiFS and adjusted using SeaBAM data,

Table 1
Laboratory estimation equation of Chl-a, TSM and CDOM.

Parameters	Equation	Explanation	References
Chl-a (μg/l)	$\frac{29.6\ (E_b - E_a)^* v}{V^* l}$	E_b = OD before adding 2M HCl, E_a = OD after adding 2M HCl, v = extracted volume of the pigment in ml, V = filtered volume of sample water in liter, l = path length of the cuvette used to measure OD in cm.	[68]
TSM (mg/L)	$\frac{(A - B) \times 1000}{C}$	A = weight of filter + dried residue, mg, B = weight of filter, mg, C = sample volume, mL.	[69]
a^{CDOM} (m^{-1})	$2.303 \times \frac{(OD_S - OD_{null})}{l}$	a^{CDOM} = absorption coefficient of CDOM, l = cuvette path length (0.01 m), 2.303 is the conversion factor of base 10 to base e (2.718) logarithms, ODS = optical density for a specific band, OD (null) = average optical density over 740–750 nm.	[70]

Table 2
Details of the Sentinel-2 MSI and Landsat-8 OLI satellite images.

Sensor	Sensing period	PRODUCT_ID	Cloud Coverage (%)
OLI	14 December 2021	LC08_L1TP_137045_20211214_20211223_01_T1	1.02
	20 March 2022	LC08_L1TP_137045_20220320_20220329_02_T1	0.29
MSI	12 December 2021	L1C_T45QYE_A024898_20211212T043524	0.18
	22 March 2022	L1C_T45QYE_A026328_20220322T043718	0.20

is a modified cubic polynomial method [73]. The OC-2 and OC-3 algorithms are well-suited for managing the diverse turbidity levels in coastal and estuarine waters, including those in the Sundarbans. In the present study, the OC-2 and OC-3 algorithms were employed to calculate Chl-a concentration by utilizing specific band ratios from two sensors, as outlined in Table-3. For OC-2, the ratio of Rrs at 490 and 555 nm was used. Conversely, OC-3 employed the higher ratio between Rrs values at 443 nm, 555 nm or 448 nm, and 555 nm [72, 73]. A regression model has been applied to estimate the TSM concentration incorporating various band combinations of reflectance values from the MSI [74] (Table 3). For TSM, the Green/NIR and Red/NIR band ratio algorithms were selected for their sensitivity to sediment concentrations, which is crucial in the highly turbid waters of the Sundarbans. C2RCC atmospheric correction is a full-spectrum version that uses neural networks trained on simulated top-of-atmosphere reflectance [75]. The C2RCC processor was specifically applied to the Landsat-8 OLI satellite sensor to estimate a^{CDOM} within the study area. It was chosen for CDOM due to its robustness in optically complex waters, effectively distinguishing between various water constituents. These algorithms were selected for their ability to address the challenges posed by the Sundarbans' dynamic estuarine ecosystem, which features significant seasonal variability and high turbidity. Specifically, they are well-suited to handle elevated levels of suspended sediments and accurately retrieve chlorophyll-a and CDOM concentrations in such complex optical environments.

2.6. Model evaluation and validation

Results have been evaluated and validated to assess the reliability and correctness of the satellite derived concentrations with in situ measurements of Chl-a, TSM and CDOM, respectively. We also considered the model's calculated and observed values, the Root Mean Square Error (RMSE) (Eqn. (1)), Bias (Eqn. (2)), Mean Absolute Percentage Error (MAPE) (Eqn. (3)), Coefficient of Determination (r) (Eqn. (4)), to be able to ascertain our model's accuracy. RMSE measures the difference between values predicted by the model and the actual values (in-situ measurements). It provides an average magnitude of the errors, with lower RMSE indicating better model performance [76]. Bias shows the systematic error between in-situ and satellite-derived values. A positive bias suggests an overestimation by the model, while a negative bias indicates underestimation [77]. MAPE measures the percentage error between in-situ and satellite-derived data. It is a normalized metric that expresses error as a percentage, providing insight into the scale of discrepancies [76].

The formula for the above statistical indices are given below:

$$RMSE = \sqrt{\frac{\sum_{i=1}^{n}\left(X_{insitu,i} - X_{sensor,i}\right)^2}{n}} \tag{1}$$

$$Bias = \frac{1}{n}\sum_{i}^{n}\left(X_{insitu,i} - X_{sensor,i}\right) \tag{2}$$

Table 3
Retrieval algorithm of Chl-a, TSM, and CDOM of the Present Study Region.

Parameters	Algorithms	Equations	Coefficient Values	References
Chl-a	OC-2	$R = \log\left(\frac{R_rs490}{R_rs555}\right)$ $C = 10^{\left(a_o + a_1 \times R + a_2 \times R^2 + a_3 \times R^3\right)} + a_4$	Where, a = 0.341, −3.0010, 2.811, −2.041, 0.0400	[45,73]
	OC-3	$R = \log\left(\frac{R_rs443 > R_rs488}{R_rs555}\right)$ $C = 10^{\left(a_o + a_1 \times R + a_2 \times R^2 + a_3 \times R^3 + a_4 \times R^4\right)}$ Note: $\left(\frac{R_rs443}{R_rs555}\right)$ or $\left(\frac{R_rs488}{R_rs555}\right)$ (which ever greater is used)	Where, a = 0.283, −2.753, 1.457, −0.659, −1.403	[45,73]
TSM	Regression Model	$X = \frac{R_rs\ Green}{R_rs\ NIR}$ TSM = ax + b	a = −12.80, b = 102.74	[74]
	Regression Model	$X = \frac{R_rs\ Red}{R_rs\ NIR}$ TSM = ax + b	a = −20.24, b = 127.08	[74]
CDOM	Neural Network	C2RCC	–	[46]

$$MAPE = \frac{1}{n}\sum_{i}^{n}\frac{\left|X_{insitu,i} - X_{sensor,i}\right|}{X_{insitu,i}} \tag{3}$$

$$r = \frac{n\sum\left(X_{insitu,i}X_{sensor,i}\right)\left(\sum X_{insitu,i}\right)\left(\sum X_{sensor,i}\right)}{\sqrt{\left[n\sum\left(X_{insitu,i}\right)^2\left(\sum X_{insitu,i}\right)^2\right]\left[n\sum\left(X_{sensor,i}\right)^2 - \left(\sum X_{sensor,i}\right)^2\right]}} \tag{4}$$

Where,

$X_{insitu,i}$ = In-situ data obtained
$X_{sensor,i}$ = Satellite data obtained
n = Sample size

3. Results

3.1. Spatial and seasonal distribution of Chl-a

The analysis of all in-situ data showed a significant difference in the seasonal mean Chl-a between the two seasons where the values ranged higher (2.3–4.36 mg/m^3) for post-monsoon than lower (1.7–4.5 mg/m^3) for pre-monsoon (Fig. 2). During the post-monsoon season, the mean Chl-a concentration was calculated at 3.04 mg/m^3, while for the pre-monsoon period, it was estimated at 2.91 mg/m^3. Spatial distribution showed that elevated Chl-a (mg/m^3) levels were identified in close proximity to the upstream and narrower areas, with a gradual decrease observed in offshore regions. Descriptive statistics detailing the estimated Chl-a concentrations are presented in Table 4.

On the other hand, Chl-a calculated from OC-2 algorithm indicated relatively higher concentrations during post-monsoon compared to pre-monsoon (Fig. 3a–b). Spatial distribution of OC-2 based outcomes for the study area indicated significant variations in Chl-a concentrations captured by the Sentinel-2 MSI sensor. Notably, the eastern part near the head of the GBM River estuary of the study area exhibited higher concentration values than the western section. Chl-a concentrations ranged from 2.5 to 5 mg/m^3 in post-monsoon (Fig. 3a), contrasting with pre-monsoon values of approximately 2–3.5 mg/m^3 (Fig. 3b). Similarly, the OC-3 algorithm for the MSI sensor also depicted distinct variations in Chl-a concentrations between the two seasons.

3.2. Spatial and seasonal distribution of TSM

The estimated TSM concentrations (mg/L) exhibited noticeable variations between the two seasons, with a higher concentration (117.5–154.5 mg/L) and having a mean of 126.04 mg/L during the pre-monsoon phase compared to lower concentration (44–113.11 mg/L) with a mean of 82.47 mg/L during post-monsoon phase (Fig. 4). It's worth mentioning that the standard deviation, coefficient of variation, and mean absolute deviation were lower during the pre-monsoon season (Table 5). Higher concentrations were particularly identified near the upstream region of both narrower and broader channels, gradually decreasing towards the downstream areas.

TSM has been shown to be difficult for remote sensing because of its multiple components [78]. The TSM model was applied to cloud-free images from Sentinel-2 MSI sensor in the tidal river system of the Sundarban Mangrove Forest during the sampling period to be able to reveal its seasonal variability and spatial distribution.

The TSM concentration was observed to be higher in the upstream region and narrower channels in compare to the wider and

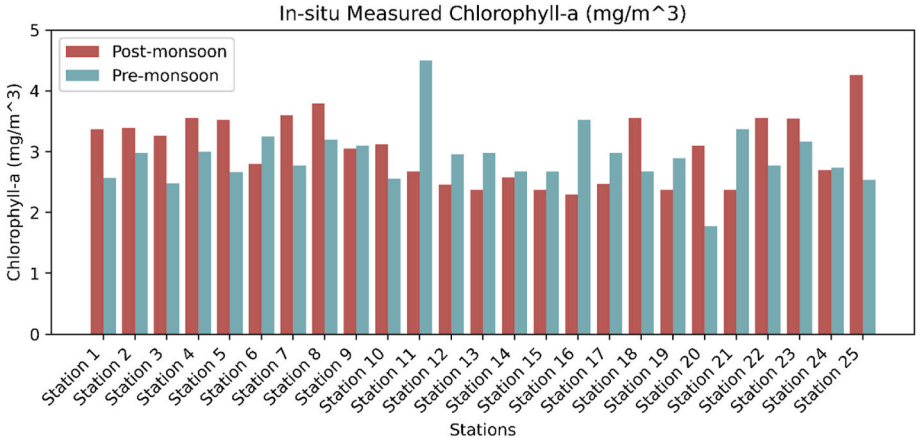

Fig. 2. In-situ measured Chl-a (mg/m^3).

Table 4
Descriptive statistics for the estimated concentrations of Chl-a.

Sampling Time	No. of Samples	Max.	Min.	Mean	Median	Mode	MAD	SD	Variance	C.V. (%)
Post-monsoon (December 2021)	25	4.36	2.3	3.04	3.1	2.37	0.48	0.56	0.31	18.30
Pre-monsoon (April 2022)	25	4.5	1.7	2.91	2.89	2.98	0.32	0.48	0.23	16.56

Note: C.V. is the coefficient of variation; SD is the standard deviation; MAD is the mean absolute deviation.

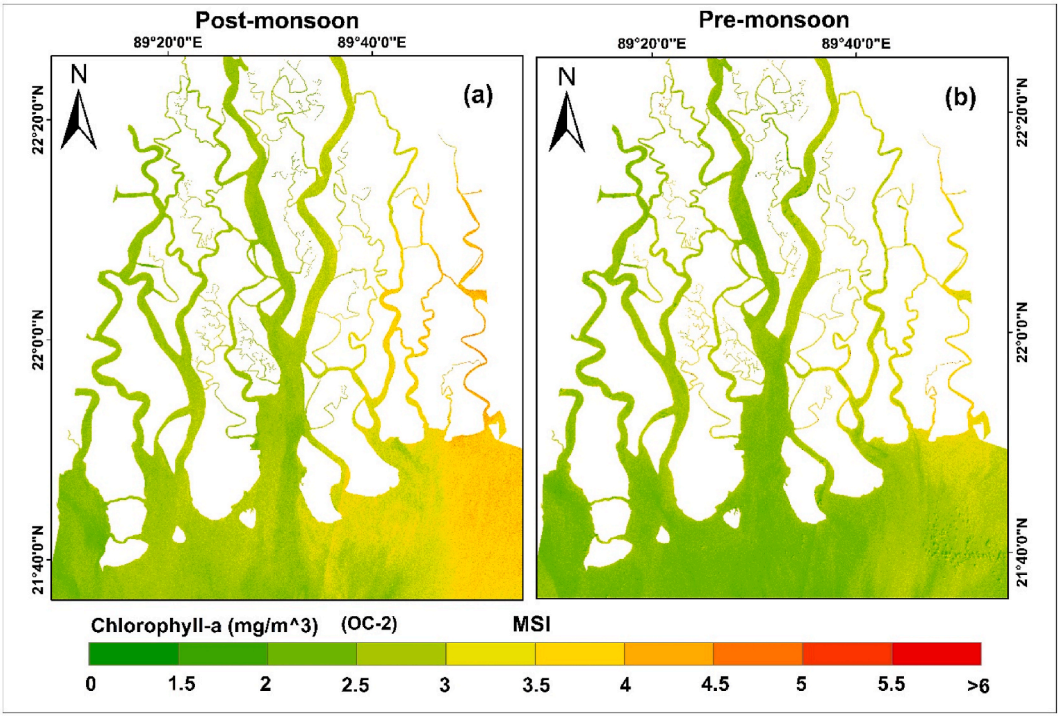

Fig. 3. Chl-a retrieved from Sentinel-2 MSI using OC-2 algorithm for (a) Post-monsoon (b) Pre-monsoon.

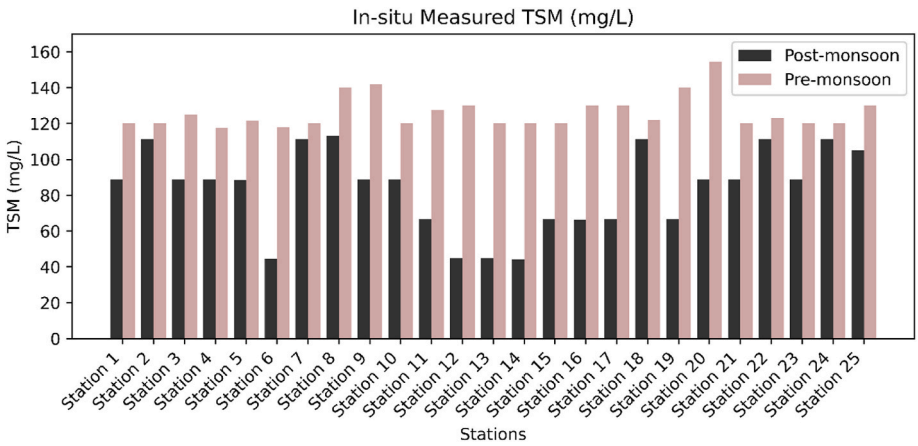

Fig. 4. Variation of in-situ TSM concentration (mg/L).

offshore areas (Fig. 5a–b). The distribution of TSM concentrations during the pre-monsoon season exhibited the highest values (80–110 mg/L) (Fig. 5a) compared to post-monsoon (75–90 mg/L) (Fig. 5b). In particularly, a decrease in TSM concentration was observed near the river mouth, with further declines in the offshore areas (5–50 mg/L).

Table 5
Descriptive statistics for the measured concentrations of TSM.

Sampling Time	No. of Samples	Max	Min	Mean	Median	MAD	SD	Variance	C.V. (%)
Post-monsoon (December 2021)	25	113.11	44	82.47	88.89	19.25	23.24	539.98	28.27
Pre-monsoon (April 2022)	25	154.5	117.5	126.04	121.5	7.17	9.28	86.21	7.36

Note: C.V. is the coefficient of variation; SD is the standard deviation; MAD is the mean absolute deviation.

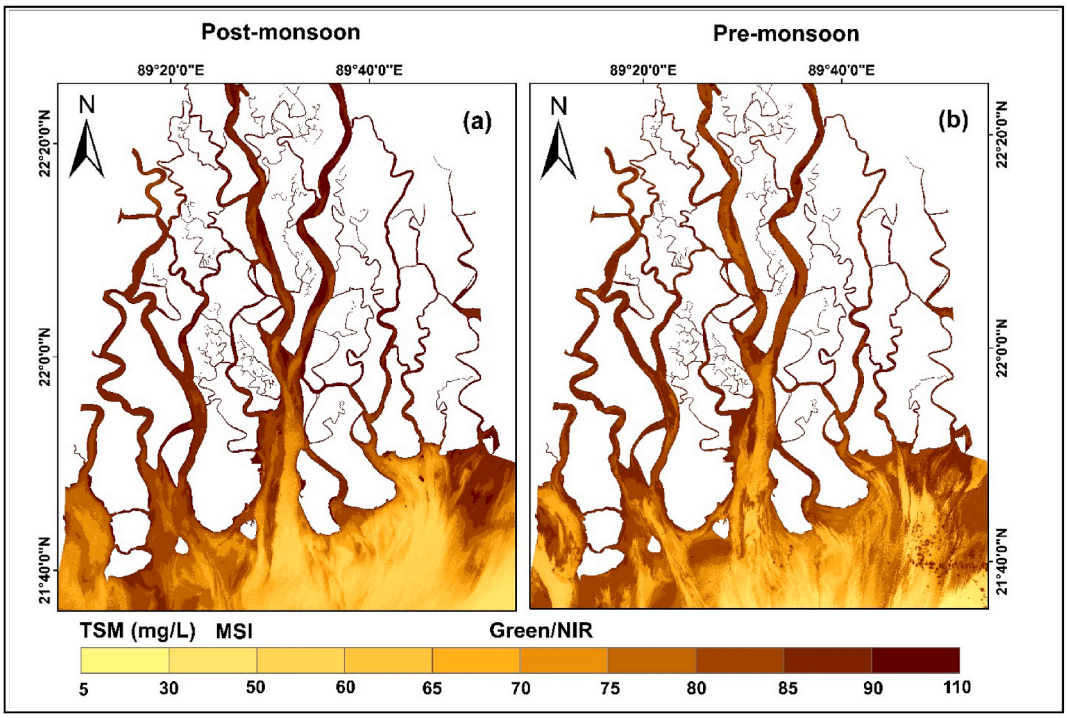

Fig. 5. Spatial and temporal distribution of TSM (a) Post-monsoon (b) Pre-monsoon.

3.3. Spatial and seasonal distribution of a^{CDOM} 443 (m^{-1})

Since the primary Chl-a absorption band is located nearby at a wavelength of 443 nm, the absorption coefficient of CDOM was specifically set for this wavelength [79]. As a result, measurements of CDOM at this wavelength may be immediately applied in remote sensing applications. The absorption coefficient of CDOM at 443 nm (a^{CDOM} m^{-1}) exhibited significant variability during two seasons,

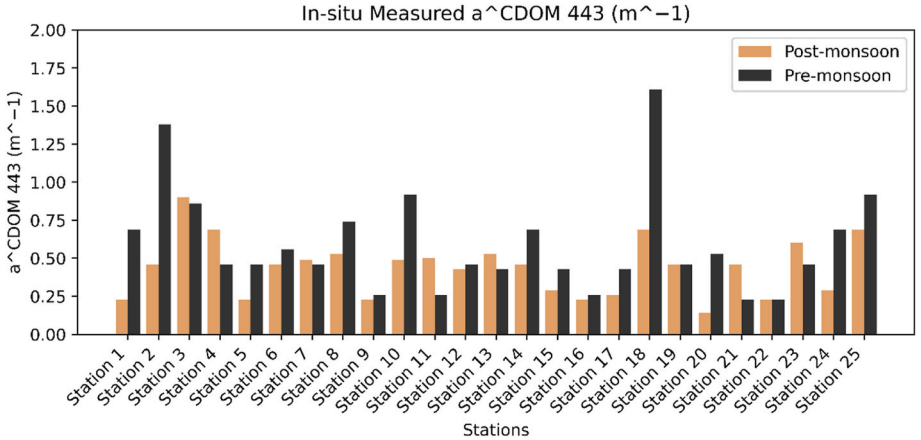

Fig. 6. Variation of in-situ measured a^{CDOM} 443 (m^{-1}).

with values ranging from 0.13 to 0.890 m^{-1} for post-monsoon and 0.23–1.62 m^{-1} for pre-monsoon. The temporal mean a^{CDOM} (443) also supported a significant difference between the two seasons. Pre-monsoon is the most important time for the seasonal dynamics of the absorption coefficient of colored dissolved organic materials at 443 nm (Fig. 6). In terms of spatial distribution, higher a^{CDOM} (443) values were observed in proximity to the upstream sampling stations, gradually decreasing in offshore areas (Fig. 7a–b). For the post-monsoon season, the mean value of a^{CDOM} (m^{-1}) is 0.439 m^{-1}, contrasting with 0.596 m^{-1} for the pre-monsoon. The minimum and maximum values for post-monsoon are lower compared to those for the pre-monsoon (Table 6).

The results revealed that the a^{CDOM} at the 443 nm wavelength in the study area was higher in the eastern region compared to the western region (Fig. 7a–b). In the rivers of the Sundarbans, the satellite-derived a^{CDOM} ranged between 0.02 and 0.99 m^{-1} in post-monsoon (Figs. 7a), 0.1 and 4 m^{-1} in the pre-monsoon season (Fig. 7b).

3.4. Comparison of Chl-a, TSM and a^{CDOM} 443 using earth observation and in-situ data

Accurate assessment of satellite-derived Chl-a concentrations relies heavily on the precision of bio-optical algorithms and validation is crucial for ensuring the reliability [32]. For the post-monsoon and pre-monsoon seasons, data from 25 stations were used for validation. Pointwise water leaving reflectance pixel values were extracted and compared with in-situ datasets. The validation result indicates that using OC-2 algorithm for MSI sensor showed the highest coefficient of determination, $R^2 = 0.73$, and the prediction accuracy RMSE = 0.27 mg/m^3; MAPE = 7%; Bias = 0.09 mg/m^3 during post-monsoon season (Fig. 8a). On the other hand, the OC-2 showed moderate correlation which is around $R^2 = 0.55$ the prediction accuracy RMSE = 0.32 mg/m^3; MAPE = 6%; Bias = −0.07 mg/m^3 during the pre-monsoon season. OC-3 retrieval algorithm for Chl-a concentration performed lesser than OC-2 retrieval algorithm (Fig. 8b) where bias is also higher.

Several algorithms, including empirical, semi-empirical, analytical, and semi-analytical methods, have been utilized to measure TSM concentrations through satellite-based models [80–82]. This study employed a regression model to estimate TSM concentration, utilizing various band combinations of Sentinel-2 MSI band reflectance values. To determine the most accurate prediction, the study validates the correlation between in-situ data and satellite-derived data for different bands or band ratios. In Fig. 9a, the Green/NIR band ratio algorithm exhibited highest performance in post-monsoon with a R^2 value of 0.77, and precise predictions: RMSE of 15.82 mg/L, MAPE at 15%, and a slight bias of −2.69 mg/L. Conversely, during the pre-monsoon season, the Green/NIR algorithm displayed lower performance, with a R^2 of approximately 0.65, and less accurate predictions: RMSE of 33.96 mg/L, MAPE at 36%, and a bias of 33.29 mg/L (Fig. 9b). The band ratio algorithm for Red/NIR showed the coefficient of determination, $R^2 = 0.67$, and the prediction accuracy RMSE = 21.25 mg/L; MAPE = 18%; Bias = -13.58 mg/L during post-monsoon (Fig. 9c). The model showed correlation for the Red/NIR algorithm, which is around $R^2 = 0.62$ for both sensors; the prediction accuracy RMSE = 19.70 mg/L; MAPE = 18%; Bias = 18.81 mg/L during the pre-monsoon season (see Fig. 9d). The Green/NIR band ratio algorithm performed better compared to the Red/NIR band ratio based algorithm for the present study area.

One of the most important measures of the health of coastal ecosystems is the capacity of coastal waters to allow sunlight to reach planktonic, macro-phytic, and other submerged vegetation for photosynthesis [70]. So, health of the ecosystem in the present study

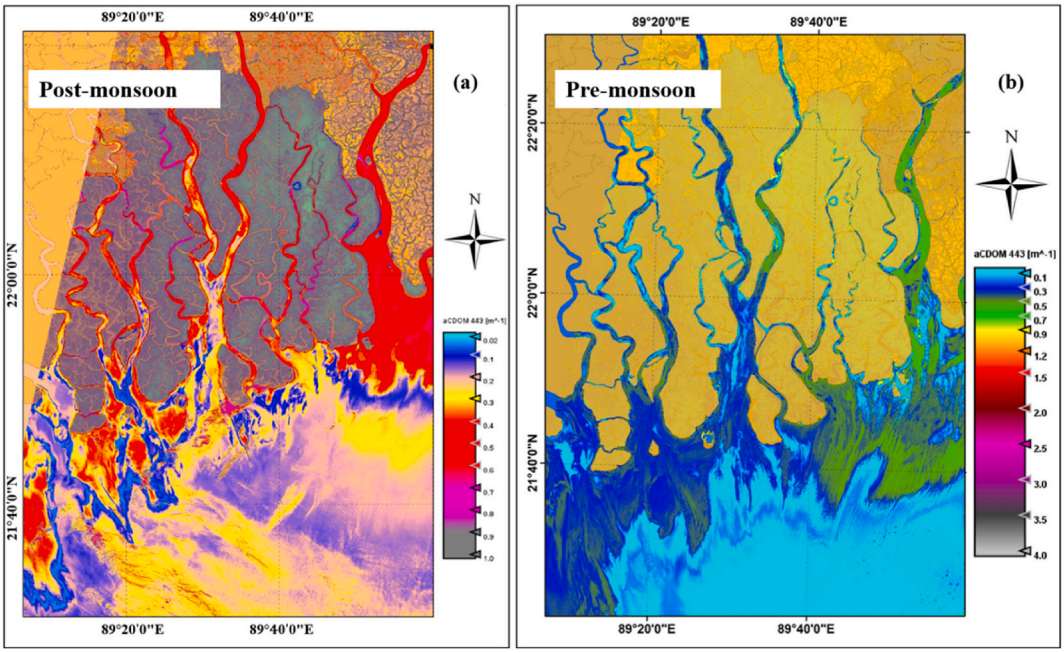

Fig. 7. Spatial and temporal distribution of satellite derived a^{CDOM} at 443 nm (a) Post-monsoon (b) Pre-monsoon.

Table 6
Descriptive Statistics of In-situ a^{CDOM} m^{-1} at 443 nm.

Sampling Time	No. of Samples	Max	Min	Mean	Median	Mode	MAD	SD	Variance	C.V. (%)
Post-monsoon (December 2021)	25	0.898	0.139	0.439	0.461	0.461	0.146	0.187	0.035	42.56
Pre-monsoon (April 2022)	25	1.612	0.230	0.596	0.461	0.461	0.252	0.341	0.116	57.14

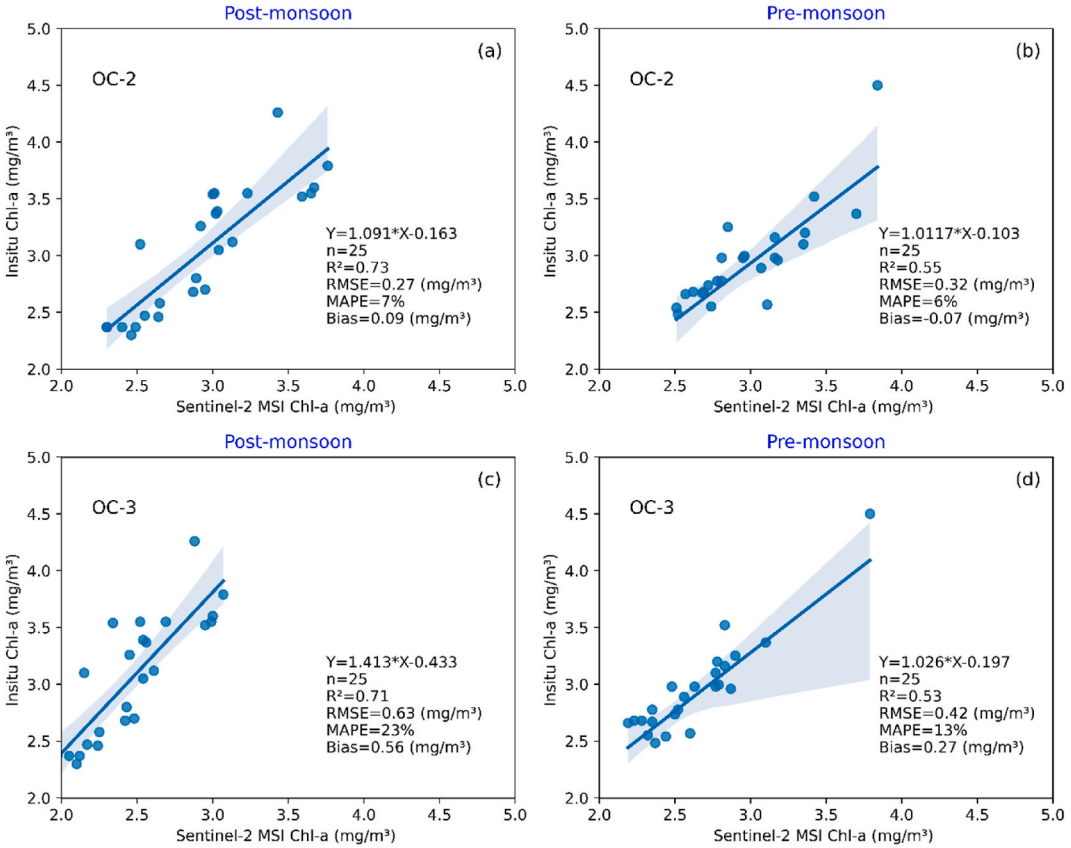

Fig. 8. Scatter plot displaying Chl-a concentrations (a) In-situ Chl-a (mg/m^3) Vs Sentinel-2 MSI derived Chl-a for Post-monsoon and (b) for Pre-Monsoon season using OC-2 algorithm (c) In-situ Chl-a (mg/m^3) Vs Sentinel-2 MSI derived Chl-a for Post-monsoon and (d) for Pre-Monsoon season using OC-3 algorithm.

area is dependent on the absorption properties of CDOM because this region is important for fisheries production. The variability of a^{CDOM} (443) is very rarely documented in the surface waters of the Sundarban mangroves forest. After matchup with in-situ data with the satellite derived a^{CDOM} (using C2RCC) for post-monsoon season the coefficient of determination, $R^2 = 0.74$, and the prediction accuracy RMSE = 0.12 m^{-1}; MAPE = 33% and Bias = 0.05 m^{-1} (Fig. 10a). For the season of Pre-monsoon, coefficient of determination $R^2 = 0.55$ and the prediction accuracy RMSE = 0.26 m^{-1}; MAPE = 83%; and Bias = 0.13 m^{-1} (Fig. 10b). For the post-monsoon season the prediction accuracy MAPE is good as it is <30% compared to the pre-monsoon season where the prediction accuracy is bad. Higher CDOM concentrations were observed in the study region during the pre-monsoon season compared to post-monsoon, possibly originating from land sources or organic decompositions.

4. Discussion

This study investigated spatial distribution and seasonal variation of three major water quality parameter's: Chl-a, TSM, and CDOM in world's largest mangrove aquatic system using Earth observation data: Sentinel-2 MSI and Landsat-8 OLI and subsequently validated with the in-situ data. According to our research, there were notable variations in the concentration and spatial distribution of both of these parameters throughout the studied region. As far as we are aware, no previous study has focused on the seasonal and spatial variability of significant water quality measures while examining the aquatic environment in the Sundarbans region. In this study, high concentration of Chl-a within the narrower channel and nearshore waters obtained both in-situ and satellite data during

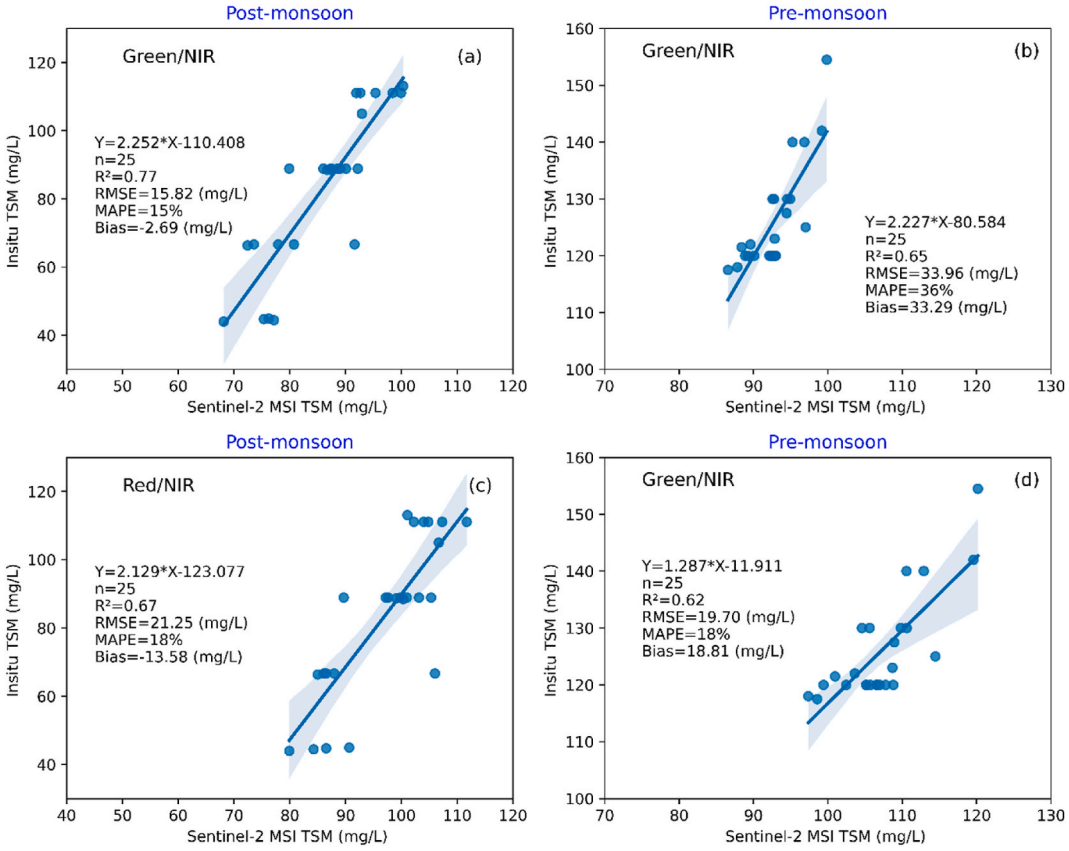

Fig. 9. Scatter plot of TSM concentrations (a) In-situ TSM (mg/L) Vs Sentinel-2 MSI derived TSM for Post-monsoon and b) for Pre-monsoon season using Green/NIR band ratio algorithm (c) In-situ TSM (mg/L) Vs Sentinel-2 MSI for Post-monsoon and d) Pre-monsoon season using Red/NIR band ratio algorithm. (For interpretation of the references to color in this figure legend, the reader is referred to the Web version of this article.)

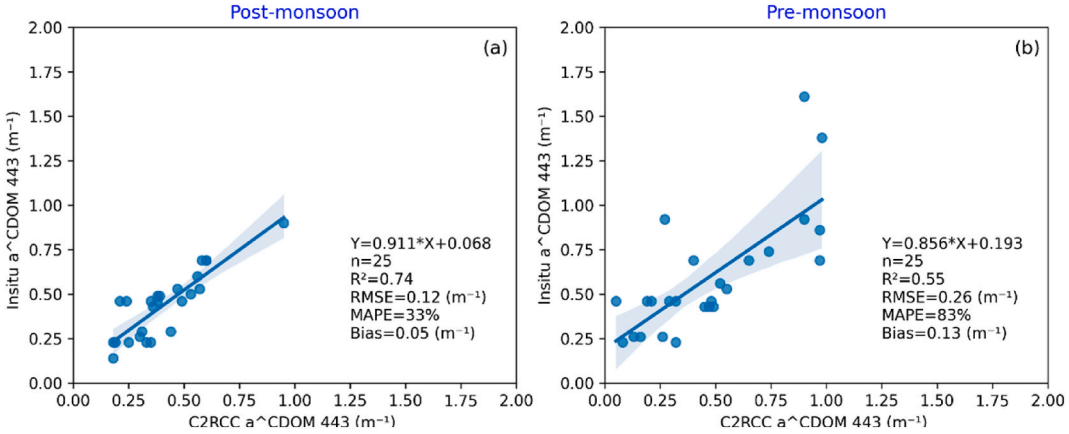

Fig. 10. Scatter plot of a^{CDOM} 443 (m^{-1}) (a) In-situ a^{CDOM} 443 (m^{-1}) Vs C2RCC derived a^{CDOM} 443 (m^{-1}) for Post-monsoon (b) In-situ a^{CDOM} 443 (m^{-1}) Vs C2RCC derived a^{CDOM} 443 (m^{-1}) for Pre-monsoon season.

post-monsoon phase which are considered to be regulated by the availability of the nutrient concentrations from land sources. The monsoon and post-monsoon seasons have the largest concentration of nutrients deposited, which promote phyto-plankton growth and, consequently, the enrichment of Chl-a [83,84]. Despite the nutrients being present in the monsoon and post-monsoon, higher concentration of Chl-a may be observed during the post-monsoon because of the favorable water temperatures and the pre-settled nutrients that the rivers previously transported [45]. Phytoplankton production typically occurs in cooler waters, and the elevated Chl-a levels observed during the post-monsoon season in our study area can be attributed to this phenomenon. Plankton growth and

distribution rely on environmental carrying capacity, inorganic nutrient availability, and coastal water physicochemical characteristics [85]. The fluctuation in nutrient concentration was primarily a result of freshwater inflow from perennial rivers and monsoon rainfall, as well as anthropogenic factors [86]. Moreover, nutrients concentration is significantly influenced by precipitation. Shafeeque et al. (2019) [87] in their study showed that given the positive correlation between Chl-a and precipitation, the higher Chl-a concentrations during the winter (post-monsoon) season can be further attributed to increased precipitation. Higher monthly total precipitations during post-monsoon can lead to increased nutrient transport, contributing to elevated Chl-a levels in the study area. In the study area, the monthly average precipitation in post-monsoon (December) (Fig. 11a) was higher compared to pre-monsoon (April) (see Fig. 11b).

In our study, the eastern part near the head of the Ganges-Brahmaputra-Meghna (GBM) river estuary had higher Chl-a concentration values than the western section (see Fig. 3a–b). However, high Chl-a levels are limited to the head of the GBM River estuary in the post-monsoon and pre-monsoon. This phenomenon could be attributed due to the GBM delta river system, which transports ecologically and nutrient enriched waters in the northern BoB [18]. Hoq et al. (2006) [88] reported that fluctuating Chl-a levels in the Sundarbans, with lower values recorded during the pre-monsoon and monsoon seasons in Koyra, Kholpatua, and Madar rivers and elevated Chl-a values were observed during the post-monsoon seasons. Observations from Rahman et al. (2014) [1] study also supported this claim regarding the higher Chl-a concentrations in the Sundarban area during post-monsoon period. We found that, Chl-a concentrations derived from earth observation data indicated that OC-2 exhibited higher prediction accuracy and overall better performance compared to the OC-3 algorithm. Studies elsewhere such as Poddar et al. (2019) [45] also observed that the OC-2 algorithm provides a Chl-a estimate with a higher correlation of 0.795 and minimal bias of 0.35 mg/m^3. Whilst Lotliker et al. (2019) [32] obtained R^2 values of 0.67 and 0.50 in the western BoB using the OC-3 algorithm with MODIS and VIIRS, respectively.

Both seasonal and spatial variabilities observed in the TSM concentrations in the coastal water of the Sundarban mangrove forest. Its changes are highly dynamical, spatial, and seasonal in the northern coastal BoB [89]. There are number of factors namely turbidity, organic inorganic matters, chlorophyll concentration, waste water dilution, and the tidal fluctuations that govern TSM fluctuation in the study area [90]. However, all these factors are largely influenced by tidal action as the study area is highly tidal dominated that varies spatially and temporally. Higher TSM levels were reported in upstream areas, with distinct variations in estimated concentrations within larger and smaller channels. This might result due to the fact that enormous quantities of sediments are carried downstream by river discharge and are deposited in the channel, with the remainder being discharged into the BoB near Sundarban area [91]. Human activities like channel dredging significantly influence variations of TSM concentrations in estuaries. Where the complex structure, along with channel deepening and stretching, contributes to higher bank erosion and suspended sediment concentrations [91]. The fluctuation in TSM concentration illustrates the impact of the summer monsoon on river runoff and its subsequent influence on TSM concentration [89]. Both river runoff and tidal forces, exerting a significant influence at the study site, contribute to variations in TSM concentration [92–94]. Wind energy is one of the important variables that plays a role in the resuspension of sediment [95]. a distinct spatial and temporal variation, such as a higher concentration at the river mouth during the pre-monsoon period, are observed. This occurrence is attributed to elevated wind speeds during that time, leading the re-suspension of sediments. It is evident from the monthly average wind speed that was found higher during pre-monsoon (Fig. 12b) compared to the post-monsoon (Fig. 12a).

Transparency measurements in this study showed a considerable rise in the post-monsoon compared to the pre-monsoon season, when increase turbidity resulted in decreased transparency. Dust deposition in the ocean and river discharge, which carry TSM from terrestrial sources, have an impact on the spread of TSM [96]. Regarding this assumption, we found a negative correlation between secchi disk depth and TSM concentrations (Fig. 13a–b), with transparency being greater downstream compared to upstream channels.

In the Northern BoB, a^{CDOM} values exhibited seasonal variations, increasing in the pre-monsoon, and decreasing after the monsoon. In spatial analysis, higher values of a^{CDOM} were observed nearshore areas, gradually decreasing offshore. The a^{CDOM} (m^{-1}) concentration varies with in-situ and ex-situ sources, which means it can be from terrestrial or marine sources. In the current study area, pre-monsoon concentrations were found to be greater, and this finding may be explained by marine sources. The elevated wind speed during the pre-monsoon season suggests that resuspension processes may contribute to the increased CDOM levels in the study area. a^{CDOM} (443) levels peaked at the end of summer, declining as the post-monsoon months approached and water flow became limited, as reported by Das et al. (2016) [97]. It is anticipated that CDOM would fluctuate greatly across time and place due to the complicated optical nature of the study area. Human activities, such as discharging domestic or industrial effluents into rivers, and the in-situ creation from phytoplankton debris, contribute to elevated CDOM concentrations in coastal waters [98,99]. Additionally, the mixing of freshwater and saltwater, along with environmental factors like photo-degradation in coastal areas, leads to changes in CDOM's optical characteristics [70,98–102]. The absorption coefficient of CDOM (a^{CDOM}) had a significant inverse linear connection with the salinity of the surface waters, which suggests the presence of the conventional mixing effect of marine and fresh water [70]. Several other studies found similar relationship between Sea Surface Salinity (SSS) and a^{CDOM} [103,104]. As SSS increase during the post-monsoon due to lower discharge of freshwater the a^{CDOM} decreased accordingly [70]. Pandi et al. (2014) [105] also found a significant inverse liner relationship with SSS in their study. The present study also found negative correlation between a^{CDOM} and SSS (Table 7). In our study, we have not had any significant correlation between a^{CDOM} and Chl-a or TSM (Fig. 14a–f) which was quite analogous to the finding of Das et al. (2017) [70]. Knowing the sources and sinks of CDOM is essential to comprehending the carbon cycle and biogeochemical activities that include CDOM directly or indirectly. These processes are more prevalent in coastal and estuarine systems than in offshore areas [106]. Building on this study, there are several potential areas for future research. Future research could explore additional water quality parameters, such as dissolved oxygen, turbidity, total organic carbon, alkalinity, hardness, metals, and nutrients etc., to provide a more comprehensive view of the ecosystem. Investigating the impact of climate change on water quality and applying advanced machine learning techniques for improved data accuracy are also promising areas.

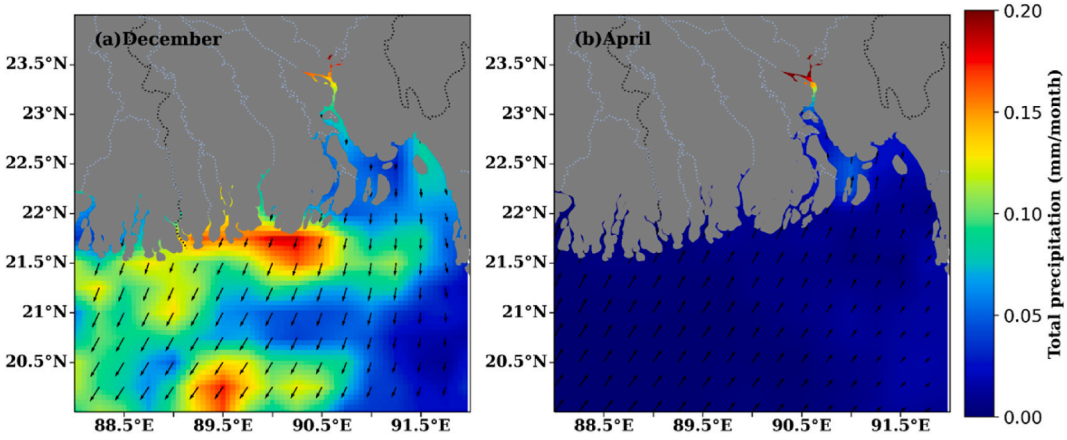

Fig. 11. Monthly average precipitation during (a) Post-monsoon (b) Pre-monsoon in the study area.

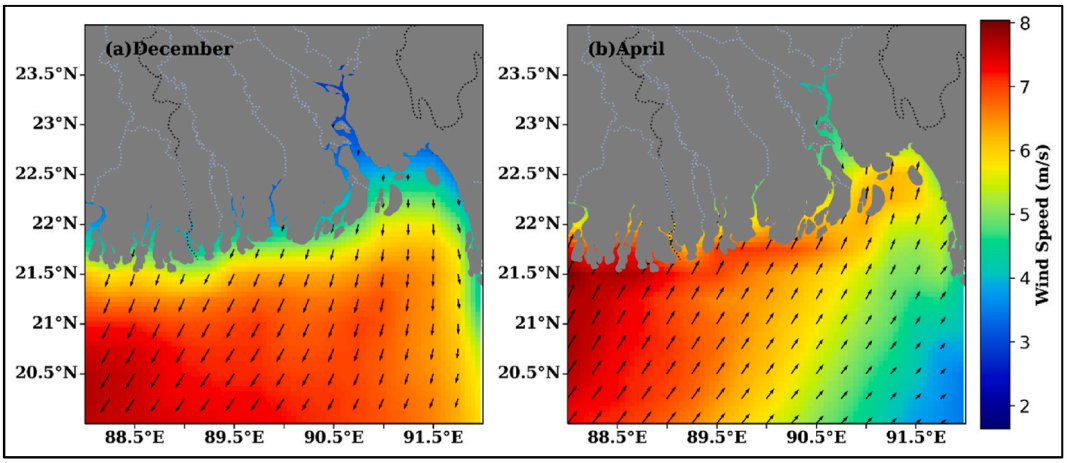

Fig. 12. Wind speed (m/s) with their direction during (a) Post-monsoon and (b) Pre-monsoon.

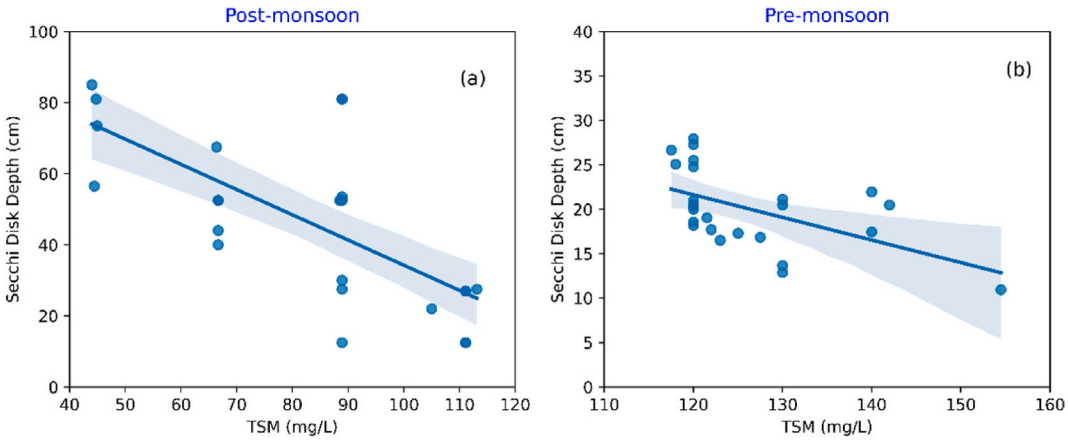

Fig. 13. Relationship between TSM and Secchi disk depth (a) Post-monsoon (b) Pre-monsoon.

Therefore, the findings will contribute to develop management and preservation plans by highlighting the spatial and seasonal variability of water quality in the Sundarbans. Based on these results, we recommend adaptive water quality monitoring using remote sensing to promptly address changes, sustainable resource management to regulate human activities like fishing and tourism, and

Table 7
Correlations between a^{CDOM} (443) and related variables.

Variables	a^{CDOM}	
	Post-monsoon	**Pre-monsoon**
SSS	−0.30	−0.26
TSM	0.10	−0.12
Chl-a	0.34	−0.35
Turbidity	0.3	0.05

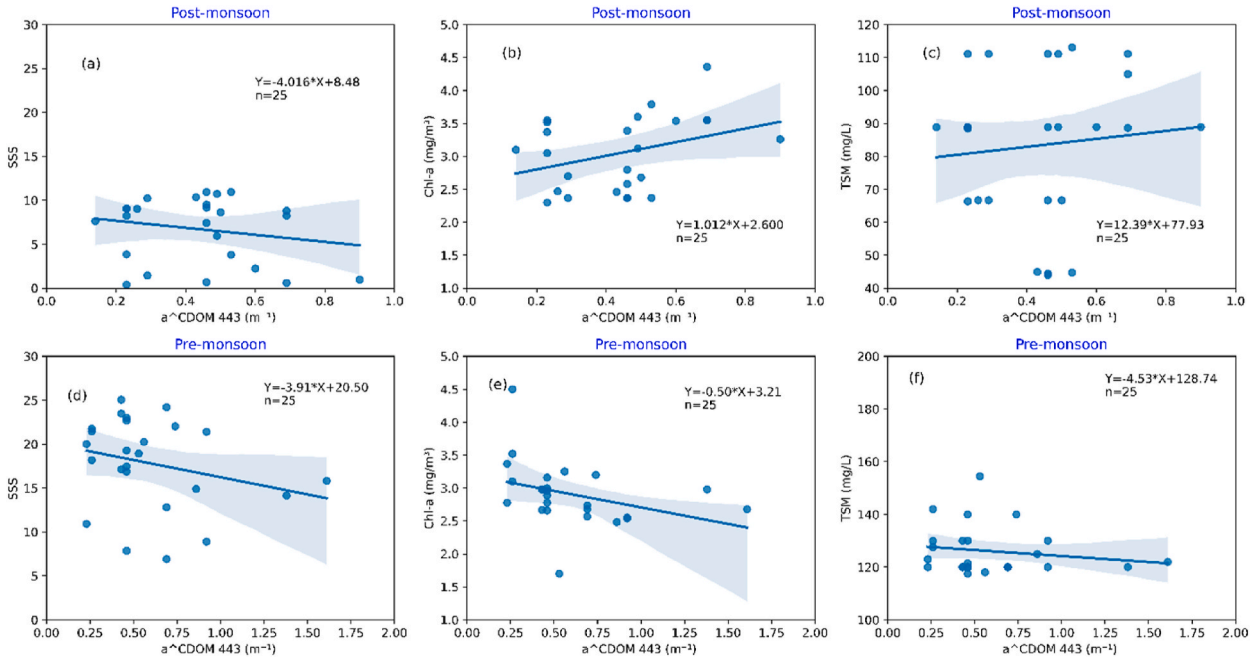

Fig. 14. Correlation between a^{CDOM} 443 (m^{-1}) with SSS (a, d), Chl-a (b, e), and TSM (c, f) for both post-monsoon and Pre-monsoon season, respectively.

climate change mitigation policies to address impacts such as sea level rise and increased salinity. These strategies will support the long-term preservation of the Sundarbans ecosystem. Long-term studies using time-series satellite data could further enhance understanding of seasonal and inter-annual variability in the Sundarbans.

5. Conclusion

The present study examines three crucial water quality measures utilizing multispectral satellites imagery namely Sentinel-2 MSI and Landsat-8 OLI sensors to assess performance and calculate seasonal and spatial variability in the intricate network of tidal rivers that make up the Sundarban Mangrove Forest. The study utilized OC-2 and OC-3 retrieval algorithms to estimate Chl-a concentrations from Sentinel-2 MSI satellite imagery. Following a comparison with in-situ measured Chl-a, the OC-2 algorithm demonstrated higher accuracy. For TSM estimation, Green/NIR and Red/NIR band ratio regression algorithms were employed, with the Green/NIR regression exhibiting higher prediction accuracy. Additionally, the C2RCC processor was applied to derive absorption coefficients of CDOM (a^{CDOM}) from Landsat-8 OLI satellite data. The result showed a significant seasonal and spatial variation in the present study area. Chl-a, TSM, and CDOM are highly dominated in the upstream narrower channels compared to the downstream and wider channels. During the post-monsoon season, Chl-a concentrations were higher than in the pre-monsoon, while TSM and CDOM concentrations were elevated during the pre-monsoon season. Factors influencing Chl-a concentration included favorable water temperature, pre-deposited nutrient concentrations, and precipitation. TSM concentration was influenced by wind speed, regulating the resuspension process, leading to higher TSM concentrations during the pre-monsoon season, where elevated wind speeds were observed. CDOM concentration was also higher during the pre-monsoon, attributed to intensified sediment resuspension processes driven by higher wind speeds, accompanied by an influx of freshwater reducing surface salinity and contributing to higher a^{CDOM} concentrations. This study initiated the use of earth observation data to estimate critical water quality parameters in the Sundarban mangrove forest of Bangladesh. By assessing seasonal and spatial variations in Chl-a, sunlight penetration (influenced by TSM and CDOM), the research aims to gauge the impact of anthropogenic threats on primary productivity, ecosystem health, environmental

change, and water quality. This information is pivotal for prioritizing areas that need immediate conservation attention and developing targeted management strategies. It also supports the creation of policies that adapt to the changing environmental conditions in the Sundarbans, such as establishing seasonal monitoring programs, promoting sustainable fishing practices to prevent overfishing, implementing habitat restoration projects to improve water quality and biodiversity, and implementing conservation measures tailored to the region's specific ecological needs throughout the year. The findings will also contribute to sustainable fishing practices, ecosystem management, and pollution prevention, aligning with SDG 14.1 and 14.2 objectives. However, this study did not invent new algorithms; instead, it applied established algorithms from relevant studies adapted to the region. By leveraging these existing algorithms, the research will help to assess the present conditions and productivity of the world's largest mangrove ecosystems. To strengthen the prediction of these light-sensitive parameters, it is necessary to build regional algorithms that require greater sample frequencies.

Data availability

Data will be made available on request.

CRediT authorship contribution statement

Mosa. Tania Alim Shampa: Writing – original draft, Visualization, Validation, Software, Methodology, Investigation, Formal analysis, Conceptualization. **Md. Kawser Ahmed:** Validation, Supervision, Resources, Conceptualization. **K. M. Azam Chowdhury:** Validation, Supervision, Resources. **Md. Ashraful Islam:** Writing – review & editing, Visualization, Methodology, Data curation. **Mahmudul Hasan:** Writing – review & editing, Visualization, Supervision, Project administration, Methodology, Investigation, Funding acquisition, Conceptualization. **Muhammad Shahinur Rahman:** Visualization, Software, Resources, Methodology, Data curation. **Md. Saiful Islam:** Writing – review & editing, Visualization, Resources.

Declaration of competing interest

The authors declare the following financial interests/personal relationships which may be considered as potential competing interests:Mahmudul Hasan reports financial support was provided by University of Dhaka. Md. Kawser Ahmed reports financial support was provided by University of Dhaka. If there are other authors, they declare that they have no known competing financial interests or personal relationships that could have appeared to influence the work reported in this paper.

Acknowledgements

We express our gratitude to the Centennial Research Grant (CRG) (2020–2021) from the University of Dhaka, Bangladesh; the Ministry of Science and Technology of the People's Republic of Bangladesh for awarding the National Science and Technology (NST) fellowship,and the International Center for Ocean Governance (ICOG), for their generous financial support that was essential for the successful completion of our research. Special thanks also go to the Department of Oceanography, the Department of Botany, and the Centre for Advanced Research in Sciences (CARS) at the University of Dhaka for their invaluable assistance in facilitating the proper conduct of laboratory analyses for this research project.

References

[1] F. Rahman, M.T. Rahman, M.S. Rahman, J.U. Ahmed, Organic production of koromjol, Passur river system of the sundarbans, Bangladesh, Asian J. Water Environ. Pollut. 11 (2014) 95–103. https://journals.sagepub.com/doi/pdf/10.3233/AJW-2014-11_1_11.
[2] S.M.B. Rahaman, L. Sarder, M.S. Rahaman, A.K. Ghosh, S.K. Biswas, S.S. Siraj, K.A. Huq, A.F.M. Hasanuzzaman, S.S. Islam, Nutrient dynamics in the Sundarbans mangrove estuarine system of Bangladesh under different weather and tidal cycles, Ecol Process 2 (2013) 29, https://doi.org/10.1186/2192-1709-2-29.
[3] H. Mahmood, M. Ahmed, T. Islam, M.Z. Uddin, Z.U. Ahmed, C. Saha, Paradigm shift in the management of the Sundarbans mangrove forest of Bangladesh: issues and challenges, Trees, Forests and People 5 (2021) 100094, https://doi.org/10.1016/j.tfp.2021.100094.
[4] S.M.D.-U. Islam, M.A.H. Bhuiyan, Sundarbans mangrove forest of Bangladesh: causes of degradation and sustainable management options, Environmental Sustainability 1 (2018) 113–131, https://doi.org/10.1007/s42398-018-0018-y.
[5] MdH. Iqbal, Valuing ecosystem services of Sundarbans Mangrove forest: approach of choice experiment, Global Ecology and Conservation 24 (2020) e01273, https://doi.org/10.1016/j.gecco.2020.e01273.
[6] R.N. Mandal, P. Saenger, C.S. Das, A. Aziz, Current status of mangrove forests in the trans-boundary sundarbans, in: H.S. Sen (Ed.), The Sundarbans: A Disaster-Prone Eco-Region, Springer International Publishing, Cham, 2019, pp. 93–131, https://doi.org/10.1007/978-3-030-00680-8_4.
[7] MdS. Islam, M. Haque, The mangrove-based coastal and nearshore fisheries of Bangladesh: ecology, exploitation and management, Rev. Fish Biol. Fish. 14 (2004) 153–180, https://doi.org/10.1007/s11160-004-3769-8.
[8] M.M. Hoque Mozumder, MdM. Shamsuzzaman, Md Rashed-Un-Nabi, E. Karim, Social-ecological dynamics of the small scale fisheries in Sundarban Mangrove Forest, Bangladesh, Aquaculture and Fisheries 3 (2018) 38–49, https://doi.org/10.1016/j.aaf.2017.12.002.
[9] S.K. Sarkar, A.K. Bhattacharya, Conservation of biodiversity of the coastal resources of Sundarbans, Northeast India: an integrated approach through environmental education, Mar. Pollut. Bull. 47 (2003) 260–264, https://doi.org/10.1016/S0025-326X(02)00475-7.
[10] M.M. Islam, Poverty in Small-Scale Fishing Communities in Bangladesh: Contexts and Responses, 2012 urn:nbn:de:gbv:46-00102866-18.
[11] M. Getzner, M. Shariful Islam, Natural resources, livelihoods, and reserve management: a case study from sundarbans mangrove forests, Bangladesh, Int. J. SDP 8 (2013) 75–87, https://doi.org/10.2495/SDP-V8-N1-75-87.
[12] G.T. Nguyen, N.T.H. Huynh, Seasonal variations in groundwater quality under different impacts using statistical approaches, Civ. Eng. J 9 (2023) 497–511, https://doi.org/10.28991/CEJ-2023-09-03-01.

[13] A. Chowdhury, S.K. Maiti, Assessing the ecological health risk in a conserved mangrove ecosystem due to heavy metal pollution: a case study from Sundarbans Biosphere Reserve, India, Hum. Ecol. Risk Assess. 22 (2016) 1519–1541, https://doi.org/10.1080/10807039.2016.1190636.

[14] S.B. Neogi, M. Dey, S.L. Kabir, S.J.H. Masum, G. Kopprio, S. Yamasaki, R. Lara, Sundarban mangroves: diversity, ecosystem services and climate change impacts, Asian J. Med. Biol. Res 2 (2017) 488–507, https://doi.org/10.3329/ajmbr.v2i4.30988.

[15] H.W. Paerl, Assessing and managing nutrient-enhanced eutrophication in estuarine and coastal waters: interactive effects of human and climatic perturbations, Ecol. Eng. 26 (2006) 40–54, https://doi.org/10.1016/j.ecoleng.2005.09.006.

[16] M.F. Chislock, E. Doster, R.A. Zitomer, A.E. Wilson, Eutrophication: causes, consequences, and controls in aquatic ecosystems, Nature Education Knowledge 4 (10) (2013). https://www.wilsonlab.com/wp-content/uploads/2021/05/2013_NE_Chislock_et_al.pdf.

[17] M.R.H. Khondoker, K.R. Hasan, Waste management of a maritime port-the case of Mongla port authority, J. Nav. Architect. Mar. Eng. 17 (2020) 219–230, https://doi.org/10.3329/jname.v17i2.48925.

[18] M.M. Rahman, Marine environmental pollution in Bangladesh and it's protection, International Journal of Research Publication and Reviews 2 (2021) 993–1003. https://ijrpr.com/uploads/V2ISSUE10/IJRPR1607.pdf.

[19] A.H. Chowdhury, M.A. Akber, Study of impacts of oil spill on the Sundarbans mangrove forest of Bangladesh, Journal of the Asiatic Society of Bangladesh, Science 41 (2015) 75–94, https://doi.org/10.3329/jasbs.v41i1.46193.

[20] M. Gholizadeh, A. Melesse, L. Reddi, A comprehensive review on water quality parameters estimation using remote sensing techniques, Sensors 16 (2016) 1298, https://doi.org/10.3390/s16081298.

[21] D. Tang, H. Kawamura, M.-A. Lee, T. Van Dien, Seasonal and spatial distribution of chlorophyll-a concentrations and water conditions in the Gulf of Tonkin, South China Sea, Rem. Sens. Environ. 85 (2003) 475–483, https://doi.org/10.1016/S0034-4257(03)00049-X.

[22] L. Tian, O. Wai, X. Chen, Y. Liu, L. Feng, J. Li, J. Huang, Assessment of total suspended sediment distribution under varying tidal conditions in deep Bay: initial results from HJ-1A/1B satellite CCD images, Rem. Sens. 6 (2014) 9911–9929, https://doi.org/10.3390/rs6109911.

[23] Y. Deng, Y. Zhang, B. Lemos, H. Ren, Tissue accumulation of microplastics in mice and biomarker responses suggest widespread health risks of exposure, Sci. Rep. 7 (2017) 46687, https://doi.org/10.1038/srep46687.

[24] Z. Lee, C. Hu, S. Shang, K. Du, M. Lewis, R. Arnone, R. Brewin, Penetration of UV-visible solar radiation in the global oceans: insights from ocean color remote sensing, JGR Oceans 118 (2013) 4241–4255, https://doi.org/10.1002/jgrc.20308.

[25] X. Liu, Y. Zhang, K. Shi, Y. Zhou, X. Tang, G. Zhu, B. Qin, Mapping aquatic vegetation in a large, shallow eutrophic lake: a frequency-based approach using multiple years of MODIS data, Rem. Sens. 7 (2015) 10295–10320, https://doi.org/10.3390/rs70810295.

[26] C.A. Stedmon, S. Markager, H. Kaas, Optical properties and signatures of chromophoric dissolved organic matter (CDOM) in Danish coastal waters, Estuar. Coast Shelf Sci. 51 (2000) 267–278, https://doi.org/10.1006/ecss.2000.0645.

[27] N.V. Blough, R. Del Vecchio, Chromophoric DOM in the coastal environment, in: Biogeochemistry of Marine Dissolved Organic Matter, Elsevier, 2002, pp. 509–546, https://doi.org/10.1016/B978-012323841-2/50012-9.

[28] S. Singh, E.J. D'Sa, E.M. Swenson, Chromophoric dissolved organic matter (CDOM) variability in Barataria Basin using excitation–emission matrix (EEM) fluorescence and parallel factor analysis (PARAFAC), Sci. Total Environ. 408 (2010) 3211–3222, https://doi.org/10.1016/j.scitotenv.2010.03.044.

[29] D. Pozdnyakov, R. Shuchman, A. Korosov, C. Hatt, Operational algorithm for the retrieval of water quality in the Great Lakes, Rem. Sens. Environ. 97 (2005) 352–370, https://doi.org/10.1016/j.rse.2005.04.018.

[30] O.C. Montanher, E.M.L.M. Novo, C.C.F. Barbosa, C.D. Rennó, T.S.F. Silva, Empirical models for estimating the suspended sediment concentration in Amazonian white water rivers using Landsat 5/TM, Int. J. Appl. Earth Obs. Geoinf. 29 (2014) 67–77, https://doi.org/10.1016/j.jag.2014.01.001.

[31] E. Chassot, S. Bonhommeau, G. Reygondeau, K. Nieto, J.J. Polovina, M. Huret, N.K. Dulvy, H. Demarcq, Satellite remote sensing for an ecosystem approach to fisheries management, ICES (Int. Counc. Explor. Sea) J. Mar. Sci. 68 (2011) 651–666, https://doi.org/10.1093/icesjms/fsq195.

[32] A.A. Lotiker, T.S. Kumar, V.S. Reddem, S. Nayak, Cyclone Phailin enhanced the productivity following its passage: evidence from satellite data. Current Science, Current Science Association 106 (n.d.) 360–361. https://repository.ias.ac.in/103610/1/0360.pdf.

[33] A. Syarif Sukri, S. M, R. Karama, Nasrul, R. Talanipa, A. Kadir, N.H. Aswad, Utilization management to ensure clean water sources in coastal areas, J. Hum. Earth Future 4 (2023) 23–35, https://doi.org/10.28991/HEF-2023-04-01-03.

[34] V. Theenathayalan, S. Sathyendranath, G. Kulk, N. Menon, G. George, A. Abdulaziz, N. Selmes, R. Brewin, A. Rajendran, S. Xavier, T. Platt, Regional satellite algorithms to estimate chlorophyll-a and total suspended matter concentrations in vembanad lake, Rem. Sens. 14 (2022) 6404, https://doi.org/10.3390/rs14246404.

[35] A.N. Tyler, P.D. Hunter, E. Spyrakos, S. Groom, A.M. Constantinescu, J. Kitchen, Developments in Earth observation for the assessment and monitoring of inland, transitional, coastal and shelf-sea waters, Sci. Total Environ. 572 (2016) 1307–1321, https://doi.org/10.1016/j.scitotenv.2016.01.020.

[36] E. Ghaderpour, A. Ben Abbes, M. Rhif, S.D. Pagiatakis, I.R. Farah, Non-stationary and unequally spaced NDVI time series analyses by the LSWAVE software, Int. J. Rem. Sens. 41 (2020) 2374–2390, https://doi.org/10.1080/01431161.2019.1688419.

[37] Y.A. Nanehkaran, B. Chen, A. Cemiloglu, J. Chen, S. Anwar, M. Azarafza, R. Derakhshani, Riverside landslide susceptibility overview: leveraging artificial neural networks and machine learning in accordance with the united nations (UN) sustainable development goals, Water 15 (2023) 2707, https://doi.org/10.3390/w15152707.

[38] M.E. Power, N. Brozović, C. Bode, D. Zilberman, Spatially explicit tools for understanding and sustaining inland water ecosystems, Front. Ecol. Environ. 3 (2005) 47–55, https://doi.org/10.1890/1540-9295(2005)003[0047:SETFUA]2.0.CO;2.

[39] J.C. Ritchie, P.V. Zimba, J.H. Everitt, Remote sensing techniques to assess water quality, Photogramm Eng Remote Sensing 69 (2003) 695–704, https://doi.org/10.14358/PERS.69.6.695.

[40] F. Mohseni, F. Saba, S.M. Mirmazloumi, M. Amani, M. Mokhtarzade, S. Jamali, S. Mahdavi, Ocean water quality monitoring using remote sensing techniques: a review, Mar. Environ. Res. 180 (2022) 105701, https://doi.org/10.1016/j.marenvres.2022.105701.

[41] E. Valentini, F. Filipponi, A. Nguyen Xuan, F. Passarelli, A. Taramelli, Earth observation for maritime spatial planning: measuring, observing and modeling marine environment to assess potential aquaculture sites, Sustainability 8 (2016) 519, https://doi.org/10.3390/su8060519.

[42] R. Adrian, D. Gerten, V. Huber, C. Wagner, S.R. Schmidt, Windows of change: temporal scale of analysis is decisive to detect ecosystem responses to climate change, Mar Biol 159 (2012) 2533–2542, https://doi.org/10.1007/s00227-012-1938-1.

[43] S. Hermawan, D. Bangguna, E. Mihardja, J. Fernaldi, J.E. Prajogo, The hydrodynamic model application for future coastal zone development in remote area, Civ. Eng. J 9 (2023) 1828–1850, https://doi.org/10.28991/CEJ-2023-09-08-02.

[44] R. Lawford, A. Strauch, D. Toll, B. Fekete, D. Cripe, Earth observations for global water security, Curr. Opin. Environ. Sustain. 5 (2013) 633–643, https://doi.org/10.1016/j.cosust.2013.11.009.

[45] S. Poddar, N. Chacko, D. Swain, Estimation of chlorophyll-a in northern coastal Bay of bengal using landsat-8 OLI and sentinel-2 MSI sensors, Front. Mar. Sci. 6 (2019) 598, https://doi.org/10.3389/fmars.2019.00598.

[46] D. Kyryliuk, S. Kratzer, Evaluation of sentinel-3A OLCI products derived using the case-2 regional CoastColour processor over the Baltic Sea, Sensors 19 (2019) 3609, https://doi.org/10.3390/s19163609.

[47] V. Das, G. Kalyan, S. Hazra, M. Pal, Understanding the role of structural integrity and differential expression of integrin profiling to identify potential therapeutic targets in breast cancer, J. Cell. Physiol. 233 (2018) 168–185, https://doi.org/10.1002/jcp.25821.

[48] A. De, I. Mondal, S. Nandi, S. Thakur, M. Raman, T.K. De, Estimation of chlorophyll-a, SPM and salinity in mangrove dominated tropical estuarine areas of hooghly river, north east coast of Bay of bengal, India using sentinel-3 data, 2021, https://doi.org/10.21203/rs.3.rs-1191959/v1.

[49] I. Moutzouris-Sidiris, K. Topouzelis, Assessment of chlorophyll-a retrievals algorithms from Sentinel-2 satellite data, in: K. Themistocleous, D.G. Hadjimitsis, S. Michaelides, V. Ambrosia, G. Papadavid (Eds.), Sixth International Conference on Remote Sensing and Geoinformation of the Environment (RSCy2018), SPIE, Paphos, Cyprus, 2018, p. 64, https://doi.org/10.1117/12.2326675.

[50] Y.O. Ouma, K. Noor, K. Herbert, Modelling reservoir chlorophyll- a , TSS, and turbidity using sentinel-2A MSI and landsat-8 OLI satellite sensors with empirical multivariate regression, J. Sens. 2020 (2020) 1–21, https://doi.org/10.1155/2020/8858408.

[51] J. Boucher, K.C. Weathers, H. Norouzi, B. Steele, Assessing the effectiveness of Landsat 8 chlorophyll *a* retrieval algorithms for regional freshwater monitoring, Ecol. Appl. 28 (2018) 1044–1054, https://doi.org/10.1002/eap.1708.

[52] F. Watanabe, E. Alcântara, T. Rodrigues, L. Rotta, N. Bernardo, N. Imai, Remote sensing of the chlorophyll-a based on OLI/Landsat-8 and MSI/Sentinel-2A (Barra Bonita reservoir, Brazil), An. Acad. Bras. Ciênc. 90 (2018) 1987–2000, https://doi.org/10.1590/0001-3765201720170125.

[53] P.A. Salyuk, I.E. Stepochkin, E.B. Sokolova, S.P. Pugach, V.A. Kachur, I.I. Pipko, Developing and using empirical bio-optical algorithms in the western part of the bering sea in the late summer season, Rem. Sens. 14 (2022) 5797, https://doi.org/10.3390/rs14225797.

[54] W. Zhu, S. Pang, J. Chen, N. Sun, L. Huang, Y. Zhang, Z. Zhang, S. He, Q. Cheng, Spatiotemporal variations of total suspended matter in complex archipelagic regions using a sigmoid model and Landsat-8 imagery, Regional Studies in Marine Science 36 (2020) 101308, https://doi.org/10.1016/j.rsma.2020.101308.

[55] E.S. Leggesse, F.A. Zimale, D. Sultan, T. Enku, R. Srinivasan, S.A. Tilahun, Predicting optical water quality indicators from remote sensing using machine learning algorithms in tropical highlands of Ethiopia, Hydrology 10 (2023) 110, https://doi.org/10.3390/hydrology10050110.

[56] D. Mukherjee, A.K. Paul, Mangrove sensitivities to climate change and its impacts in the Sundarbans: a case study in the Patibania Island of south western Sundarbans, India, in: Modern Cartography Series, Elsevier, 2021, pp. 353–385, https://doi.org/10.1016/B978-0-12-823895-0.00030-0.

[57] A. Aziz, A. Paul, Bangladesh sundarbans: present status of the environment and biota, Diversity 7 (2015) 242–269, https://doi.org/10.3390/d7030242.

[58] A. Chowdhury, A. Naz, S.B. Sharma, R. Dasgupta, Changes in salinity, mangrove community ecology, and organic blue carbon stock in response to cyclones at Indian sundarbans, Life 13 (2023) 1539, https://doi.org/10.3390/life13071539.

[59] H.S. Sen (Ed.), The Sundarbans: A Disaster-Prone Eco-Region: Increasing Livelihood Security, Springer International Publishing, Cham, 2019, https://doi.org/10.1007/978-3-030-00680-8.

[60] M. Rahman, M. Asaduzzaman, Ecology of sundarban, Bangladesh, J Sci Found 8 (2013) 35–47, https://doi.org/10.3329/jsf.v8i1-2.14618.

[61] M.M. Islam, M.M. Hossain, Community dependency on the ecosystem services from the sundarbans mangrove Wetland in Bangladesh, in: B.A.K. Prusty, R. Chandra, P.A. Azeez (Eds.), Wetland Science, Springer India, New Delhi, 2017, pp. 301–316, https://doi.org/10.1007/978-81-322-3715-0_16.

[62] M.I.Md Shameem, S. Momtaz, R. Rauscher, Vulnerability of rural livelihoods to multiple stressors: a case study from the southwest coastal region of Bangladesh, Ocean Coast Manag. 102 (2014) 79–87, https://doi.org/10.1016/j.ocecoaman.2014.09.002.

[63] S.A. Hussain, R. Badola, Valuing mangrove benefits: contribution of mangrove forests to local livelihoods in Bhitarkanika Conservation Area, East Coast of India, Wetlands Ecol Manage 18 (2010) 321–331, https://doi.org/10.1007/s11273-009-9173-3.

[64] DoF, YEARBOOK OF FISHERIES STATISTICS OF BANGLADESH 2019-20, Department of Fisheries, Bangladesh Ministry of Fisheries and Livestock, Government of the People's Republic of Bangladesh, 2020. 2021-09-15-09-08-6403c5da6be3f3d0250c5dcb170c5e1a.pdf.

[65] C. Inskip, M. Ridout, Z. Fahad, R. Tully, A. Barlow, C.G. Barlow, MdA. Islam, T. Roberts, D. MacMillan, Human–tiger conflict in context: risks to lives and livelihoods in the Bangladesh sundarbans, Hum. Ecol. 41 (2013) 169–186, https://doi.org/10.1007/s10745-012-9556-6.

[66] M. Hossain, M.R.H. Siddique, S.M.R. Abdullah, S. Saha, D.C. Ghosh, MdS. Rahman, S.H. Limon, Nutrient dynamics associated with leaching and microbial decomposition of four abundant mangrove species leaf litter of the sundarbans, Bangladesh, Wetlands 34 (2014) 439–448, https://doi.org/10.1007/s13157-013-0510-1.

[67] M.M. Islam, S.M. Akther, M.F. Hossain, Z. Parveen, Spatial distribution and ecological risk assessment of potentially toxic metals in the Sundarbans mangrove soils of Bangladesh, Sci. Rep. 12 (2022) 10422, https://doi.org/10.1038/s41598-022-13609-z.

[68] G.W. Marker, Why schools abandon "new social studies" materials, Theor. Res. Soc. Educ. 7 (1980) 35–57, https://doi.org/10.1080/00933104.1980.10506067.

[69] APHA, Standard Methods for the Examination of Water and Waste Water, twenty-first ed., twenty-first ed., American Public Health Association, Washington, 2005.

[70] S. Das, I. Das, S. Giri, A. Chanda, S. Maity, A.A. Lotliker, T.S. Kumar, A. Akhand, S. Hazra, Chromophoric dissolved organic matter (CDOM) variability over the continental shelf of the northern Bay of Bengal, Oceanologia 59 (2017) 271–282, https://doi.org/10.1016/j.oceano.2017.03.002.

[71] W. Moses, J. Bowles, M. Corson, Expected improvements in the quantitative remote sensing of optically complex waters with the use of an optically fast hyperspectral spectrometer—a modeling study, Sensors 15 (2015) 6152–6173, https://doi.org/10.3390/s150306152.

[72] J.E. O'Reilly, S. Maritorena, D.A. Siegel, M.C. O'Brien, D. Toole, B.G. Mitchell, M. Kahru, F.P. Chavez, P. Strutton, G.F. Cota, S.B. Hooker, C.R. McClain, K. L. Carder, F. Muller-Karger, L. Harding, A. Magnuson, D. Phinney, G.F. Moore, J. Aiken, K.R. Arrigo, R. Letelier, M. Culver, Ocean Color Chlorophyll a Algorithms for SeaWiFS, OC2 and OC4, 2000, pp. 9–23. Version 4, https://www.academia.edu/download/36421462/2000_OReilly_et_al_OC4v4_11-Chapt2.pdf.

[73] J.E. O'Reilly, S. Maritorena, B.G. Mitchell, D.A. Siegel, K.L. Carder, S.A. Garver, M. Kahru, C. McClain, Ocean color chlorophyll algorithms for SeaWiFS, J. Geophys. Res. 103 (1998) 24937–24953, https://doi.org/10.1029/98JC02160.

[74] Q. Wang, K. Song, Z. Wen, Y. Shang, S. Li, C. Fang, J. Du, F. Zhao, G. Liu, Long-term remote sensing of total suspended matter using Landsat series sensors in Hulun Lake, China, Int. J. Rem. Sens. 42 (2021) 1379–1397, https://doi.org/10.1080/01431161.2020.1829154.

[75] C. Brockmann, R. Doerffer, M. Peters, S. Kerstin, S. Embacher, A. Ruescas, Evolution of the C2RCC Neural Network for Sentinel 2 and 3 for the Retrieval of Ocean Colour Products in Normal and Extreme Optically Complex Waters, 2016, p. 740, 2016ESASP.740E.54B.

[76] D. Chicco, M.J. Warrens, G. Jurman, The coefficient of determination R-squared is more informative than SMAPE, MAE, MAPE, MSE and RMSE in regression analysis evaluation, PeerJ Computer Science 7 (2021) e623, https://doi.org/10.7717/peerj-cs.623.

[77] S. Kagone, N.M. Velpuri, K. Khand, G.B. Senay, M.R. Van Der Valk, D.J. Goode, S. Abu Hantash, T.M. Al-Momani, N. Momejian, J.R. Eggleston, Satellite precipitation bias estimation and correction using in situ observations and climatology isohyets for the MENA region, J. Arid Environ. 215 (2023) 105010, https://doi.org/10.1016/j.jaridenv.2023.105010.

[78] C. Giardino, M. Bresciani, F. Braga, I. Cazzaniga, L. De Keukelaere, E. Knaeps, V.E. Brando, Bio-optical modeling of total suspended solids, in: Bio-Optical Modeling and Remote Sensing of Inland Waters, Elsevier, 2017, pp. 129–156, https://doi.org/10.1016/B978-0-12-804644-9.00005-7.

[79] R.L. Miller, M. Belz, C.D. Castillo, R. Trzaska, Determining CDOM absorption spectra in diverse coastal environments using a multiple pathlength, liquid core waveguide system, Continent. Shelf Res. 22 (2002) 1301–1310, https://doi.org/10.1016/S0278-4343(02)00009-2.

[80] J. Chen, T. Cui, Z. Qiu, C. Lin, A three-band semi-analytical model for deriving total suspended sediment concentration from HJ-1A/CCD data in turbid coastal waters, ISPRS J. Photogrammetry Remote Sens. 93 (2014) 1–13, https://doi.org/10.1016/j.isprsjprs.2014.02.011.

[81] G. Wu, L. Liu, F. Chen, T. Fei, Developing MODIS-based retrieval models of suspended particulate matter concentration in Dongting Lake, China, Int. J. Appl. Earth Obs. Geoinf. 32 (2014) 46–53, https://doi.org/10.1016/j.jag.2014.03.025.

[82] H. Zhao, Q. Chen, N.D. Walker, Q. Zheng, H.L. MacIntyre, A study of sediment transport in a shallow estuary using MODIS imagery and particle tracking simulation, Int. J. Rem. Sens. 32 (2011) 6653–6671, https://doi.org/10.1080/01431161.2010.512938.

[83] D. Sengupta, G.N. Bharath Raj, S.S.C. Shenoi, Surface freshwater from Bay of bengal runoff and Indonesian throughflow in the tropical Indian ocean, Geophys. Res. Lett. 33 (2006) 2006GL027573, https://doi.org/10.1029/2006GL027573.

[84] S.K. Baliarsingh, A.A. Lotliker, K.C. Sahu, T. Sinivasa Kumar, Spatio-temporal distribution of chlorophyll-a in relation to physico-chemical parameters in coastal waters of the northwestern Bay of Bengal, Environ. Monit. Assess. 187 (2015) 481, https://doi.org/10.1007/s10661-015-4660-x.

[85] J.S. Pitchaikani, A.P. Lipton, Nutrients and phytoplankton dynamics in the fishing grounds off Tiruchendur coastal waters, Gulf of Mannar, India, SpringerPlus 5 (2016) 1405, https://doi.org/10.1186/s40064-016-3058-8.

[86] A.K. Choudhury, R. Pal, Phytoplankton and nutrient dynamics of shallow coastal stations at Bay of Bengal, Eastern Indian coast, Aquat. Ecol. 44 (2010) 55–71, https://doi.org/10.1007/s10452-009-9252-9.

[87] M. Shafeeque, P. Shah, T. Platt, S. Sathyendranath, N.N. Menon, A.N. Balchand, G. George, Effect of precipitation on chlorophyll-a in an upwelling dominated region along the west coast of India, J. Coast Res. 86 (2019) 218, https://doi.org/10.2112/SI86-032.1.

[88] M.E. Hoq, M.A. Wahab, M.N. Islam, Hydrographic status of sundarbans mangrove, Bangladesh with special reference to post-larvae and juveniles fish and shrimp abundance, Wetlands Ecol Manage 14 (2006) 79–93, https://doi.org/10.1007/s11273-005-2569-9.

[89] N. Chacko, C. Jayaram, Variability of total suspended matter in the northern coastal Bay of bengal as observed from satellite data, J Indian Soc Remote Sens 45 (2017) 1077–1083, https://doi.org/10.1007/s12524-016-0650-x.
[90] I. Mondal, A. De, S. Nandi, S. Thakur, M. Raman, T.K. De, Estimation of chlorophyll-a, TSM and salinity in mangrove dominated tropical estuarine areas of hooghly river, north east coast of Bay of bengal, India using sentinel-3 data, 2022, https://doi.org/10.21203/rs.3.rs-1191959/v2.
[91] C. Jayaram, R. Roy, N. Chacko, D. Swain, R. Punnana, S. Bandyopadhyay, S.B. Choudhury, D. Dutta, Anomalous reduction of the total suspended matter during the COVID-19 lockdown in the hooghly estuarine system, Front. Mar. Sci. 8 (2021) 633493, https://doi.org/10.3389/fmars.2021.633493.
[92] J. Jian, P.J. Webster, C.D. Hoyos, Large-scale controls on Ganges and Brahmaputra river discharge on intraseasonal and seasonal time-scales, Q. J. R. Meteorol. Soc. 135 (2009) 353–370, https://doi.org/10.1002/qj.384.
[93] A.K. Prasad, R.P. Singh, Chlorophyll, calcite, and suspended sediment concentrations in the Bay of Bengal and the Arabian Sea at the river mouths, Adv. Space Res. 45 (2010) 61–69, https://doi.org/10.1016/j.asr.2009.07.027.
[94] M.R. Islam, S.F. Begum, Y. Yamaguchi, K. Ogawa, Distribution of suspended sediment in the coastal sea off the Ganges–Brahmaputra River mouth: observation from TM data, J. Mar. Syst. 32 (2002) 307–321, https://doi.org/10.1016/S0924-7963(02)00045-3.
[95] M. Sato, R. Khanal, S. Uk, S. Siev, T. Sok, C. Yoshimura, Impact of wind on the spatio-temporal variation in concentration of suspended solids in tonle sap lake, Cambodia, Earth 2 (2021) 424–439, https://doi.org/10.3390/earth2030025.
[96] D. Borkman, Long-term trends in water clarity revealed by Secchi-disk measurements in lower Narragansett Bay, ICES (Int. Counc. Explor. Sea) J. Mar. Sci. 55 (1998) 668–679, https://doi.org/10.1006/jmsc.1998.0380.
[97] S. Das, S. Hazra, A.A. Lotlikar, I. Das, S. Giri, A. Chanda, A. Akhand, S. Maity, T.S. Kumar, Delineating the relationship between chromophoric dissolved organic matter (CDOM) variability and biogeochemical parameters in a shallow continental shelf, Egyptian Journal of Aquatic Research 42 (2016) 241–248, https://doi.org/10.1016/j.ejar.2016.08.001.
[98] A. Bricaud, A. Morel, L. Prieur, Absorption by dissolved organic matter of the sea (yellow substance) in the UV and visible domains1, Limnol. Oceanogr. 26 (1981) 43–53, https://doi.org/10.4319/lo.1981.26.1.0043.
[99] K.L. Carder, R.G. Steward, G.R. Harvey, P.B. Ortner, Marine humic and fulvic acids: their effects on remote sensing of ocean chlorophyll, Limnol. Oceanogr. 34 (1989) 68–81, https://doi.org/10.4319/lo.1989.34.1.0068.
[100] C.E. Del Castillo, P.G. Coble, Seasonal variability of the colored dissolved organic matter during the 1994–95 NE and SW Monsoons in the Arabian Sea, Deep Sea Res. Part II Top. Stud. Oceanogr. 47 (2000) 1563–1579, https://doi.org/10.1016/S0967-0645(99)00154-X.
[101] A. Morel, Optical modeling of the upper ocean in relation to its biogenous matter content (case I waters), J. Geophys. Res. 93 (1988) 10749–10768, https://doi.org/10.1029/JC093iC09p10749.
[102] A. Vodacek, F.E. Hogel, R.N. Swift, J.K. Yungel, E.T. Peltzer, N.V. Blough, The use of in situ and airborne fluorescence measurements to determine UV absorption coefficients and DOC concentrations in surface waters, Limnol. Oceanogr. 40 (1995) 411–415, https://doi.org/10.4319/lo.1995.40.2.0411.
[103] T.S. Catalá, A.M. Martínez-Pérez, M. Nieto-Cid, M. Álvarez, J. Otero, M. Emelianov, I. Reche, J. Arístegui, X.A. Álvarez-Salgado, Dissolved Organic Matter (DOM) in the open Mediterranean Sea. I. Basin–wide distribution and drivers of chromophoric DOM, Prog. Oceanogr. 165 (2018) 35–51, https://doi.org/10.1016/j.pocean.2018.05.002.
[104] G.M. Ferrari, The relationship between chromophoric dissolved organic matter and dissolved organic carbon in the European Atlantic coastal area and in the West Mediterranean Sea (Gulf of Lions), Mar. Chem. 70 (2000) 339–357, https://doi.org/10.1016/S0304-4203(00)00036-0.
[105] S.R. Pandi, N.S. Sarma, C. Gundala, V.H. Naroju, A.A. Lotliker, C.C. Bajish, S.C. Tripathy, Chromophoric dissolved organic matter traces seasonally changing coastal processes in a river-influenced region of the western Bay of Bengal, Environ. Sci. Pollut. Res. 31 (2024) 49372–49392, https://doi.org/10.1007/s11356-024-34443-y.
[106] M.A. Granskog, R.W. Macdonald, C.-J. Mundy, D.G. Barber, Distribution, characteristics and potential impacts of chromophoric dissolved organic matter (CDOM) in Hudson Strait and Hudson Bay, Canada, Continent. Shelf Res. 27 (2007) 2032–2050, https://doi.org/10.1016/j.csr.2007.05.001.
[107] M.J. Alam, A.S.M.M. Kamal, M.K. Ahmed, M. Rahman, M. Hasan, S.A.R. Rahman, Nutrient and heavy metal dynamics in the coastal waters of St. Martin's island in the Bay of Bengal, Heliyon 9 (2023) e20458. https://doi.org/10.1016/j.heliyon.2023.e20458.
[108] M. Hasan, M. Rahman, A. al Ahmed, M.A. Islam, M. Rahman, Heavy metal pollution and ecological risk assessment in the surface water from a marine protected area, Swatch of No Ground, north-western part of the Bay of Bengal, Reg. Stud. Mar. Sci. 52 (2022) 102278. https://doi.org/10.1016/j.rsma.2022.102278.
[109] M.A. Hasan, R. Fayyaz, M. Rahman, M. Hasan, M.A. Islam, S.S. Shreya, Estimation of shallow water bathymetry along the northern coast of Bay of bengal: a remote sensing-based approach, Malaysian J. Geosci. 7 (2) (2023) 173–179. http://doi.org/10.26480/mjg.02.2023.173.179.